J. Fluid Mech. (2006), *vol.* 557, *pp.* 307–336.
doi:10.1017/S0022112006009785 Printed in the United Kingdom

Turbulent thermal convection over grooved plates

By G. STRINGANO, G. PASCAZIO AND R. VERZICCO

Politecnico di Bari, DIMeG and CEMeC, Via Re David 200, 70125, Bari, Italia

(Received 5 September 2005 and in revised form 17 November 2005)

Direct numerical simulations of thermal convection over grooved plates are presented and discussed, in comparison with the standard flat-plate case, in order to gain a better understanding of the altered near-wall dynamics and of the enhancement of the heat transfer. The simulations are performed in a cylindrical cell of aspect-ratio (diameter over cell height) $\Gamma = 1/2$ at fixed Prandtl number $Pr = 0.7$ with the Rayleigh number Ra ranging from 2×10^6 to 2×10^{11}. The results show an increase of heat transfer, or in non-dimensional form the Nusselt number Nu, when the mean thermal boundary-layer thickness becomes smaller than the groove height, in agreement with earlier experimental investigations available from the literature. The present increase, however, results in a steeper power law of the Nu *vs.* Ra law rather than a simple upward shift of the Nu law of the flat plate. This finding agrees with some studies, but it is at variance with others. Possible causes for this difference are discussed with the help of an electrical analogy.

1. Introduction

The classical Rayleigh–Bénard problem, in which heat transfer occurs via a fluid between two horizontal flat plates at different temperatures, has been investigated for more than a century (Bénard 1900; Rayleigh 1916) because of the many practical applications involving heat fluxes mediated by a fluid. Theoretical (see Siggia 1994 for a comprehensive review and Grossmann & Lohse 2000 for more recent literature), experimental (Castaing *et al.* 1989; Cioni, Ciliberto & Sommeria 1997; Chavanne *et al.* 1996, 2001; Niemela *et al.* 2000; among many others) and numerical (Kerr 1996; Verzicco & Camussi 2003) studies have addressed several aspects of the problem although the main concern has always been the scaling law of the heat transfer. The problem can be simply formulated by finding the relation $Nu = Nu(Ra)$ where the Nusselt number Nu is the non-dimensional heat flux and the Rayleigh number Ra is the non-dimensional temperature difference between the plates (precise definitions of Nu and Ra are given in the following sections). Although it is now clear (Grossmann & Lohse 2000, 2001) that a simple power law cannot fit the relation $Nu = Nu(Ra)$, solutions have often been proposed in the form $Nu = ARa^{\beta}$ and several studies have been devoted to the refinement or explanation of particular values of A and β.

One of the aims of applied research is to investigate the possibility of increasing the heat transfer for a given temperature difference or in other words increasing A and/or β in the relation $Nu = ARa^{\beta}$; this would lead in industry to more compact and efficient cooling and heating devices, in turn yielding energy savings and reduced costs. Few experimental and numerical studies have shown that an effective way of enhancing the heat flux is to use rough surfaces instead of smooth ones (Prasolov 1961; Fujii, Fujii &

Takeuchi 1973; Anderson & Bohn 1986; Amin 1991, 1993; Shen, Xia & Tong 1996; Du & Tong 1998, 2000; Ciliberto & Laroche 1999; Roche *et al.* 2001; Sudhakar & Arakeri 2005) and this observation has motivated the comprehension of the heat transfer mechanisms in the presence of surface roughness. Understanding heat transport over non-smooth surfaces also has important implications in geophysics and meteorology where the topography of the ground and its texture are known to produce relevant changes in the heat and momentum fluxes (Sini, Anquetin & Mestayr 1996). The study of thermal convection over rough surfaces is also interesting for the comprehension of heat transfer over smooth surfaces since every boundary becomes rough below a threshold scale and any Rayleigh–Bénard experiment aiming at investigating very high Rayleigh-number regimes (like the 'ultimate' one indicated by Kraichnan 1962) will eventually have to contend with the irregular surface of the plates.

Some of the older studies (Prasolov 1961; Fujii *et al.* 1973) considered the heat transfer around rough circular cylinders since they were motivated by the degradation of heat exchanger performance caused by the fouling of the tubes. Prasolov (1961) showed that in the turbulent range ($10^5 \leqslant Ra \leqslant 3 \times 10^6$), artificial pyramidal roughness could increase the heat transfer coefficient of a horizontal cylinder in air up to a factor of two. Fujii *et al.* (1973), in contrast, used vertical cylinders in water and several roughness shapes, always finding a negligible effect on the local heat transfer.

The numerical studies by Amin (1991, 1993) considered, respectively, vertical and horizontal isothermal surfaces and in both cases the top and bottom boundaries were ribbed with periodic rectangular elements. For the case of vertical isothermal plates, Amin found a reduction of the heat transfer, especially for aspect ratios of the domain larger than one. On the other hand, for the case of horizontal isothermal surfaces, the wall roughness increased the heat transfer up to a maximum of 57 %; all these simulations, however, were performed on two-dimensional domains, therefore, they cannot be directly compared to three-dimensional flows.

In the recent literature only a few experimental (Shen, Xia & Tong 1996; Du & Tong 1998, 2000; Ciliberto & Laroche 1999; Roche *et al.* 2001; Sudhakar & Arakeri 2005; Qiu, Xia & Tong 2005) and theoretical (Villermaux 1998) papers have dealt with thermal convection over non-smooth plates and again the emerging scenario is far from being clear (figure 1). In fact, Shen *et al.* (1996) using rough surfaces made of a regular square array of identical pyramids, found that only the prefactor A, in the relation $Nu = ARa^{\beta}$, was affected by the wall roughness and it increased by about 20 % when the thermal boundary-layer thickness ($\lambda_\theta \simeq h/(2Nu)$) became smaller than the roughness height (δ). Du & Tong (2000) obtained essentially the same results even if using pyramids heights $\delta = 9$ mm (to be compared with $\delta = 3.2$ mm of Shen *et al.* 1996), in an otherwise identical geometry the increase of A was 76 % instead of 20 %. Ciliberto & Laroche (1999) produced rough surfaces by gluing glass spheres over copper plates; the spheres had different diameters δ, within a range $\delta_m \leqslant \delta \leqslant \delta_M$, distributed according to an algebraic probability density function (p.d.f.) $P(\delta) \sim \delta^{-\xi}$ with $1 \leqslant \xi \leqslant 2$. Once again, the wall roughness was effective only when the thermal boundary layer was thinner than the maximum height δ_M and the exponent β could be augmented up to a maximum of $\beta = 0.45$ for $\xi = 1$. In the case of a single sphere diameter (δ), the exponent β was unaffected but the numerical prefactor A decreased when $\lambda_\theta < \delta$. For all cases, mono disperse and multiple sphere diameters, the value of the Nusselt number was always smaller than the corresponding value for the flat plate. The experiment of Roche *et al.* (2001) used axisymmetric V-shaped grooves on the horizontal plates and on the sidewall. Also in this case the heat transfer was affected only when λ_θ decreased below the roughness height, but in this case, the exponent

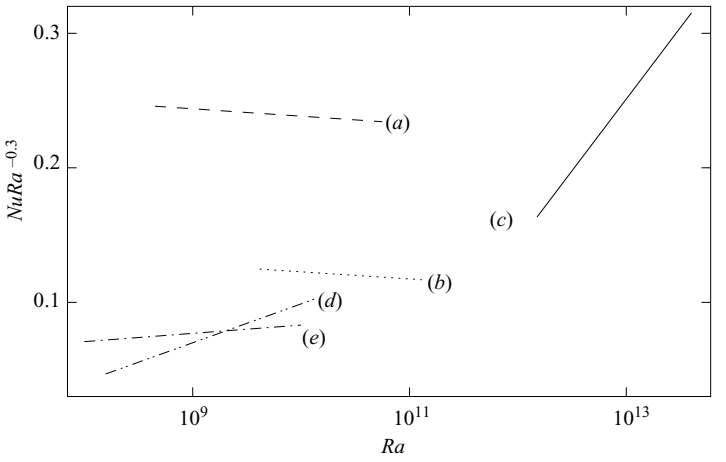

FIGURE 1. Compensated Nusselt versus Rayleigh numbers for different experiments of thermal convection over non-flat plates (only the range of Rayleigh numbers affected by the wall roughness is shown); the factor $Ra^{-0.3}$ has no particular meaning except that of reducing the scatter among the different data. (*a*) Du & Tong (2000) for $\Gamma = 0.5$, (*b*) Shen *et al.* (1996) for $\Gamma = 0.5$, (*c*) Roche *et al.* (2001), (*d*) Ciliberto & Laroche (1999) for roughness distribution with $\xi = 1$ and (*e*) Ciliberto & Laroche (1999) for $\xi = 2$. The data of Ciliberto & Laroche (1999) have been obtained in a rectangular tank for an aspect ratio $\Gamma = 2$.

β was increased up to the value $\beta = 0.51$ possibly indicating the Kraichnan (1962) ultimate regime. In this case, the effect of the wall roughness was mainly intended to alter the dependence of the viscous sublayer thickness on the Rayleigh number and therefore to neutralize the logarithmic correction factor of the power law in the Kraichnan regime.

Sudhakar & Arakeri (2005) used water as the working fluid and a rectangular tank with a bottom brass plate with straight V-shaped grooves while the upper boundary was a free surface. Their experimental procedure yielded a flow whose mean temperature increased in time, the increase, however, occurred on a time scale much longer than that of the flow unsteadiness which therefore could be treated as quasi-steady. The authors report that 'for small temperature differences' the heat transfer was the same for the smooth and grooved plates, whereas on increasing the temperature difference, the heat flux over the rough plate became larger. The different behaviours are consistent with the thinning of the thermal boundary layer for increasing Ra and the eventual crossover with the roughness height, although quantitative data are not given to verify this conjecture. Another interesting result of Sudhakar & Arakeri (2005) is that the heat transfer increase occurs through an increase of the exponent β which is different from the results of Du & Tong (2000).

Villermaux (1998) derived a theoretical model for the heat transfer assuming that the changes were essentially produced in proportion to the covering area of a sheet having uniform thickness λ_θ and laying over the rough surface. This yielded a power law $Nu \sim Ra^{\beta+\beta(d_f-2)}$ with d_f the fractal dimension of the surface roughness that, for a typical value of $d_f = 2.1$ (Feder 1988; Villermaux 1998), would give a 10 % increase in the exponent with respect to the smooth plate. For the particular case of a roughness with a single length scale δ, the surface is not fractal ($d_f = 2$) and the exponent is the same as for the smooth plate; for $\lambda_\theta \leqslant \delta$, however, there is a sudden increase of the covering area giving an analogous increase in the heat transfer.

Apart from the common finding that the surface roughness, becomes active only when the thermal boundary layer is thinner than a representative roughness height, a clear picture does not emerge from the above papers. In fact, in agreement with Villermaux (1998), for a ordered periodic roughness, Shen *et al.* (1996), Du & Tong (2000) and Ciliberto & Laroche (1999) found β to be unaffected, whereas Roche *et al.* (2001) report an increase of β up to $\beta = 0.51$. On the other hand, Shen *et al.* (1996) and Du & Tong (2000) both observed Nu to be larger than the reference flat-surface value (an increase of A) while Ciliberto & Laroche (1999) reported smaller Nusselt numbers. Indeed, the work by Ciliberto & Laroche (1999) is the only one that could be compared with the prediction for fractal surfaces of Villermaux (1998) even if the poorly conducting glass spheres of the former and the ideal perfectly conducting surfaces in the model of the latter make the comparison unlikely. On the other hand, the hypothesis of Villermaux (1998) that Nu increases only according to the coverage area of the thermal boundary layer does not find complete experimental confirmation in Du & Tong (2000) who observed the tip of the rough elements to be active points for the release of thermal plumes. The change in the dynamics was quantitatively confirmed by a Nusselt number increase of 76 % which could not be explained only in terms of area variation that at most could amount to 41 %.

A possible difference among the mentioned studies could be the thermal conductivity of the plates (copper for Roche *et al.* 2001, brass for Shen *et al.* 1996 and Du & Tong 2000 and copper with glass spheres for Ciliberto & Laroche 1999) which is already known to play a non-negligible role for smooth surfaces (Chillà *et al.* 2004; Verzicco 2004; Brown *et al.* 2005) and the effect could be exacerbated in the presence of rough elements. The shape of these elements, on the other hand, is also very different since Ciliberto & Laroche (1999) used spheres, Shen *et al.* (1996) and Du & Tong (2000) had a square array of pyramids and Roche *et al.* (2001) used axisymmetric V-shaped grooves. Other differences are the Prandtl number, the cell aspect-ratio and cell shape that can all work together to give slightly different results. Another cause of concern is the Rayleigh-number variation within each experiment; in fact, except for Roche *et al.* (2001) (in which anyway the Prandtl number changed from $Pr = 0.7$ to $Pr = 4.9$ over eleven decades of Ra), none of the mentioned experiments spanned more than two decades of Ra within the same set-up. Considering that sometimes part of this range is occupied by the Nusselt-number transition across $\lambda_\theta = \delta$, it becomes difficult to distinguish among different power laws over short ranges of Ra; this is particularly true in those experiments where the roughness height is not mono disperse since, as noted by Roche *et al.* (2001), a transition spread over several roughness heights might mimic an increased exponent.

These considerations motivated us in performing a detailed study of thermal convection over non-smooth plates within highly controlled conditions and over a wide range of Rayleigh numbers (five decades). We have performed, in particular, direct numerical simulations under the ideal condition of infinite thermal conductivity of the plates with single-height V-shaped axisymmetric grooves. This was done in an attempt to isolate first the effect of the non-smooth geometry and to compare the near-wall dynamics with that occurring over flat surfaces. The effect of the finite conductivity of the plates in the presence of grooved plates is under investigation and it will be presented in a forthcoming paper.

As an aside, we wish to stress that concerning the near-wall turbulence, Jiménez (2004) suggests that a boundary behaves as a rough surface when the height δ is of the order of, or smaller than, $\lambda_v/50$, where λ_v is the viscous boundary-layer thickness, since in this case the effect of the roughness is limited to the viscous

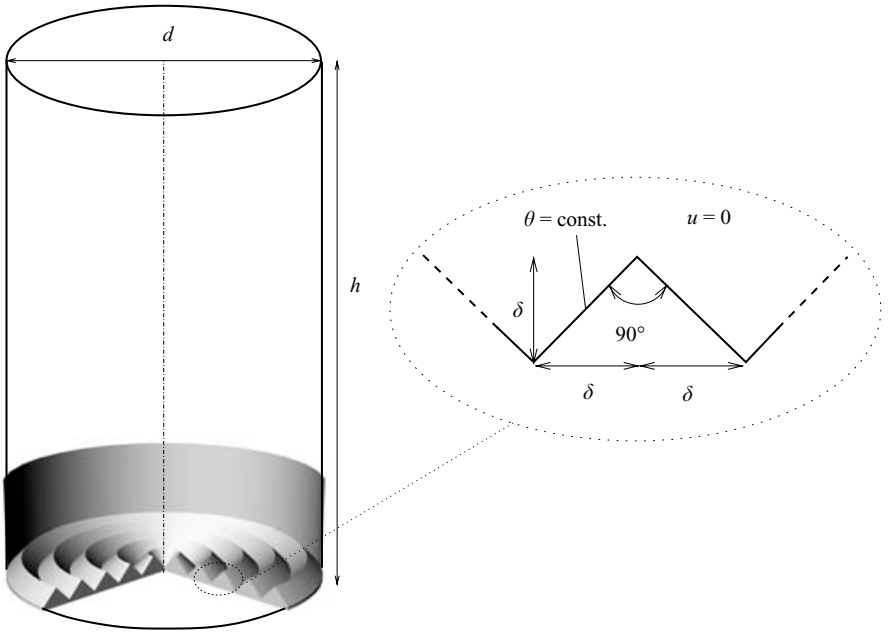

FIGURE 2. Perspective sketch of the cell and detail of the groove geometry.

and the buffer layers while the logarithmic region survives. In contrast, when the roughness is bigger, its effect extends across all the boundary layer, little is left of the original wall dynamics and the flow tends to 'see' the rough element as an obstacle. In thermal convection, the additional scale λ_θ should also be considered, nevertheless, since in the papers mentioned, the Prandtl number $0.7 \leqslant Pr \leqslant 5$, λ_θ and λ_v are of the same order of magnitude and neither in the experimental study nor in the present numerical simulations does the condition $\lambda_v/\delta \geqslant 50$ apply. This is the reason why we preferred in the title the word 'grooved' instead of 'rough' which is more commonly used.

2. Numerical method

In this paper, we simulate the flow developing in a cylindrical cell vertically confined by grooved plates, the lower being hotter than the upper (respectively, at temperatures T_h and T_c). The flow is bounded laterally by a smooth adiabatic sidewall and all the surfaces are no-slip. The grooves of the horizontal plates are V-shaped with a tip angle of 90° and with height δ (figure 2). For all the simulations, the value $\delta = 0.025h$ has been used since it is very close to the value of Du & Tong (2000) for an analogous cell and, in addition it conveniently fixes the transition $\lambda_\theta = \delta$ within our range of Rayleigh numbers (see § 2.1). The cell has a diameter-over-height aspect ratio $\Gamma = d/h = 1/2$ implying that the upper and lower plates are paved by $N = 5$ axisymmetric grooves (figure 2).

The numerical method is essentially the same as Verzicco & Orlandi (1996), Verzicco & Camussi (2003) and Verzicco (2004) where details of the numerical method and validation tests are described. The code solves the Navier–Stokes equations with

the Boussinesq approximation

$$\frac{\mathrm{D}\boldsymbol{u}}{\mathrm{D}t} = -\nabla p + \theta\hat{z} + \left(\frac{Pr}{Ra}\right)^{1/2}\nabla^2\boldsymbol{u}, \quad \nabla\cdot\boldsymbol{u} = 0, \tag{2.1a, b}$$

$$\frac{\mathrm{D}\theta}{\mathrm{D}t} = \frac{1}{(PrRa)^{1/2}}\nabla^2\theta, \tag{2.1c}$$

where $\hat{z}$ is the axial unity vector pointing in the opposite direction with respect to gravity, $\boldsymbol{u}$ the velocity vector, p the pressure and θ the non-dimensional temperature. The equations have been made non-dimensional using the free-fall velocity $U = \sqrt{g\alpha\Delta h}$, the base-to-base distance between hot and cold plates h and their temperature difference $\Delta = T_h - T_c$, therefore the Rayleigh and Prandtl numbers are, respectively, $Ra = g\alpha\Delta h^3/(\nu k)$ and $Pr = \nu/k$ with g the acceleration due to gravity, α the isobaric thermal expansion coefficient, ν the kinematic viscosity and k the thermal diffusivity of the fluid. The non-dimensional temperature θ is defined as $\theta = (T - T_c)/\Delta$ so that $0 \leqslant \theta \leqslant 1$.

The above equations have been written in a cylindrical coordinate frame and discretized on a staggered mesh by central second-order accurate finite-difference approximations. The time advancement of the solution is obtained by a hybrid low-storage third-order Runge–Kutta scheme. The algebraic system resulting from the discretized equations (2.1) has been solved by a fractional-step procedure with the elliptic equation inverted using trigonometric expansions in the azimuthal direction and the FISHPACK package (Swartzrauber 1974) for the other two directions. OpenMP directives in the code allowed the use of multi-processor shared-memory computers which turned out to be mandatory for the three-dimensional high-Rayleigh-number computations. An immersed boundary procedure (Fadlun *et al.* 2000) was already implemented in (2.1*a*) by Verzicco (2002) in order to solve momentum and temperature fields over different portions of the computational domain. In the present study, the immersed boundary procedure (IB) has been extended also to the temperature equation thus allowing the imposition of the temperature boundary condition directly on the wet surface of the grooved plates. Details about the implementation of the immersed boundary procedure, its second-order spatial accuracy and fields of application can be found in Fadlun *et al.* (2000) and Iaccarino & Verzicco (2003). Here it suffices to mention that the main advantage consists of solving flows bounded by arbitrarily complex geometries without resorting to body-conformal grids and therefore essentially with the same ease and efficiency of flows as in simple geometries. This technique has already been validated in many different contexts, however, since the IB extension to the temperature field is a new feature of the present numerical code, an additional validation test has been performed. In particular, after having computed an axisymmetric simulation at $Pr = 0.7$ and $Ra = 2 \times 10^8$ in a standard flat-plate cylindrical cell with a body-fitted mesh, the same simulation has been repeated over an extended domain with the flat plates mimicked by the IB method. The computational domains with a mean temperature field are reported in figure 3, showing a very good agreement of the results and a similar agreement was obtained for the Nusselt number resulting in $Nu = 38.49 \pm 0.75$ and $Nu = 39.21 \pm 0.95$, respectively, for the body-fitted and IB calculations.

2.1. *Grid resolution and convergence checks*

In every direct numerical simulation all the flow scales up to the smallest must be captured by an adequate grid resolution and in turbulent thermal convection these are

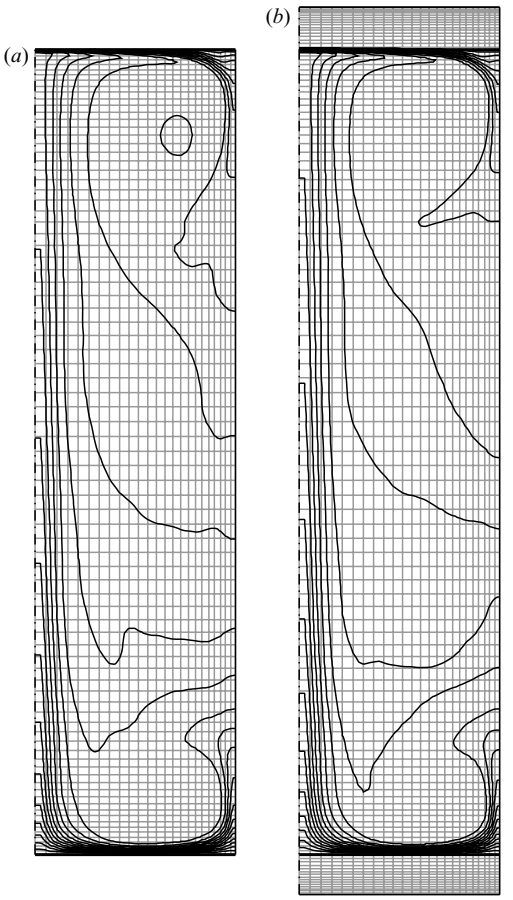

FIGURE 3. Time-averaged isothermal lines for axisymmetric simulations at $Pr = 0.7$ and $Ra = 2 \times 10^8$; the plotting stride between the contours is $\Delta\theta = 0.04$. (*a*) simulation on the body fitted mesh, (*b*) simulation with the immersed boundary method. The grey lines in the background are the grid (only every other line is plotted for clarity).

the Kolmogorov (η) and the Batchelor scales (η_θ), in the bulk, and the viscous (λ_u) and thermal (λ_θ) boundary-layer thicknesses close to the plates or other solid boundaries. Grötzbach (1983) gives an estimate for the Kolmogorov scale $\eta/h \simeq \pi(Pr/RaNu)^{1/4}$ from integral quantities while the relation $\lambda_\theta/h = 1/(2Nu)$ is commonly adopted for the thermal boundary layer: both of them can be used once a reliable correlation for $Nu(Ra)$ is available. For η_θ and λ_u different relations should be employed. However, since in this study the Prandtl number is $O(1)$, it results in $\eta \simeq \eta_\theta$ and $\lambda_\theta \simeq \lambda_u$, therefore assessing the grid resolution for η and λ_θ is representative also for the other scales.

Verzicco & Camussi (2003) used the experimental fit $Nu = 0.124Ra^{0.309}$ from Niemela *et al.* (2000) to estimate *a priori* η and λ_θ and they verified from direct measurements that the estimates were accurate enough for the determination of the grid resolution requirements. For the present problem, however, the same relations should be used with caution because a reliable correlation $Nu(Ra)$ is not available and the formula $\lambda_\theta/h = 1/(2Nu)$ has been tested only for flat-plate flows. An additional issue of the near-wall resolution is that, in the IB context, the grooved plate does

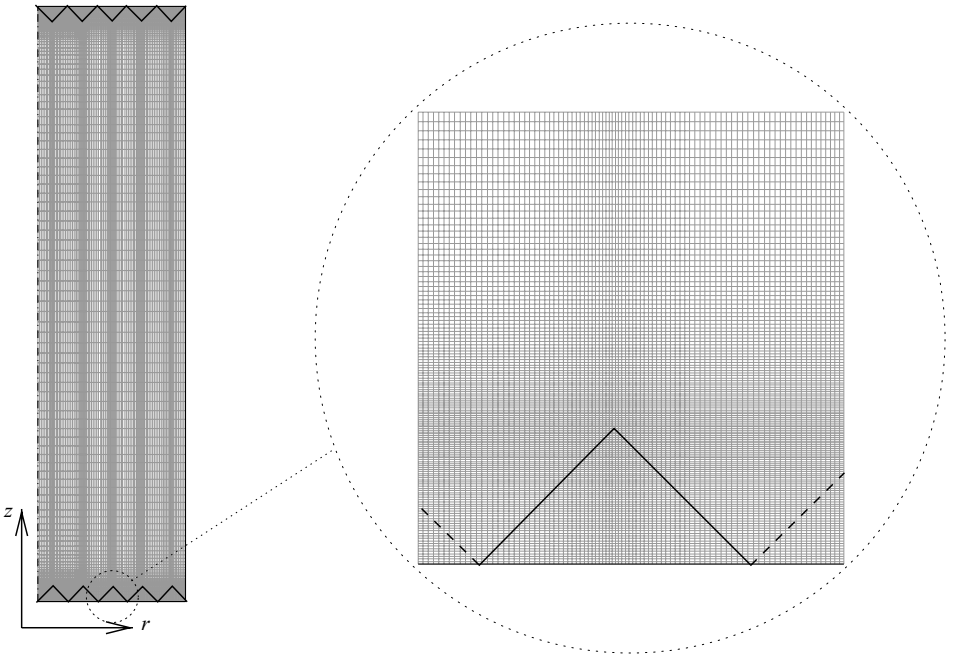

FIGURE 4. Example of mesh in a vertical meridional plane, with an enlargement of a particular groove element.

not lie over a coordinate surface. This requires that a fine spatial resolution must be maintained in the whole groove region and that the grid spacing is equally fine in the vertical and radial directions (figure 4). On account of these considerations, the only truly reliable test to assess the quality of the results is a grid refinement check in which a flow is simulated with different grids and the results are checked against each other. Unfortunately, owing to the large computational cost of the three-dimensional simulations, the grid refinement of each case was not possible. As an alternative, we have performed most of the checks over axisymmetric cases, namely two-dimensional simulations over a vertical meridional (r, z)-plane, for which the CPU time is not a limiting factor. As an example, the flow at $Ra = 2 \times 10^9$ has been computed on the grids 201×317 and 301×519 in the radial and vertical directions obtaining, respectively, the Nusselt numbers $Nu = 63.94 \pm 4.05$ and 64.85 ± 3.6; for the azimuthal resolution we used the same values as in Verzicco & Camussi (2003) since from preliminary low-Ra three-dimensional simulations (and as it could have been argued from the axisymmetric geometry of the grooves) no extra azimuthal resolution was required with respect to the flows over flat plates. As a final check, we selected the case at $Ra = 2 \times 10^8$ which is inexpensive enough to be run on different grids and we have directly verified the above criteria; in particular, we have used the grids $97 \times 151 \times 209$ and $129 \times 201 \times 301$ obtaining, respectively, $Nu = 45.88 \pm 3.05$ and $Nu = 45.57 \pm 3.35$.

According to some ongoing multiple sensor measurements in the bulk of the flow performed by P. Tong (personal communication) there is the possibility that a resolution comparable to that of the thermal boundary layer is necessary even in the bulk in order to resolve all the temperature scales; this would clearly make the numerical simulation of thermal convection unfeasible since the ratio of the bulk-to-wall grid size can also be 1000 in the high end of Ra. We believe, however, that once a plume is released from the plate it undergoes a diffusion process that progressively

Ra	$N_\theta \times N_r \times N_x$	Δ_{min}/h	Δ_{max}/h	$\frac{\overline{\lambda}_\theta}{h} = \frac{1}{(2Nu)}$	$\frac{\eta}{h} = \pi\left[\frac{Pr}{(RaNu)}\right]^{1/4}$	T
2×10^6	$65 \times 65 \times 171$	3.4×10^{-3}	8×10^{-3}	4.7×10^{-2}	4.2×10^{-2}	100
2×10^7	$97 \times 151 \times 209$	8×10^{-4}	9.8×10^{-3}	2.6×10^{-2}	2.04×10^{-2}	110
2×10^8	$97 \times 151 \times 209$	8×10^{-4}	9.8×10^{-3}	1.1×10^{-2}	9.30×10^{-3}	125
2×10^9	$129 \times 201 \times 317$	5.5×10^{-4}	5.3×10^{-3}	4.3×10^{-3}	4.14×10^{-3}	125
2×10^{10}	$129 \times 301 \times 519$	3.2×10^{-4}	4.4×10^{-3}	1.8×10^{-3}	1.88×10^{-3}	125
2×10^{11}	$193 \times 401 \times 701$	2.3×10^{-4}	3.8×10^{-3}	7.9×10^{-4}	8.57×10^{-4}	50

TABLE 1. Computational parameters of the simulations, all the computations are at $Pr = 0.7$. N_θ, N_r and N_z are, respectively, the number of nodes in the azimuthal, radial and vertical directions, T is the duration of each run in large-eddy-turnover time units. $\overline{\lambda}_\theta$ is the mean thermal boundary-layer thickness and η the estimated Kolmogorov scale. Nu is computed *a posteriori* from the simulations. Δ_{min} and Δ_{max} are, respectively, minimum and maximum grid spacing.

increases its size making it unlikely that structures in the bulk and at the wall require the same resolution. Nevertheless, the amount of diffusion depends on the flow regime (viscous or turbulent diffusion) and on the Rayleigh and Prandtl numbers, therefore for particular flow conditions it might happen that thermal plumes reach the bulk with little change in dimensions with respect to their formation. For example in high Prandtl flows ($Pr \geqslant 5$), the temperature field has a reduced diffusivity while for moderate Rayleigh numbers ($Ra \leqslant 10^{10}$), the turbulent diffusivity might not be much stronger than viscous diffusion; in these conditions indeed thermal plumes in the bulk might be similar to those of the wall region and the above resolution requirements might be necessary. This should be verified by *ad hoc* numerical tests that, however, are beyond the scope of the present paper in which the Prandtl number is kept fixed to $Pr = 0.7$.

Some details of the numerical parameters are summarized in table 1 that, compared with the analogous table of Verzicco & Camussi (2003) evidence, for a given Ra, an increase in the number of grid points by a factor 4; the total computational overhead, however, amounts to more than a factor of 10 upon considering that a finer mesh requires a proportionally smaller time step. Given the very rapid increase of the computational requirements with the Rayleigh number, we had to resort to parallel computing at $Ra = 2 \times 10^9$ and on account of the available computational resources the simulations could be scaled up to $Ra = 2 \times 10^{11}$.

In order to obtain converged statistics, each simulation was run for at least 100 large-eddy-turnover times ($T \simeq 2h/U$) which turned out to be enough at least for second-order statistics such as r.m.s. profiles and spectra. The run at $Ra = 2 \times 10^{11}$ was the only exception because of its very high computational cost; in particular, it was run for 50 large-eddy-turnover times only to obtain a reliable value of the Nusselt number. It is worth mentioning that in an experimental set-up like that of Du & Tong (2000) at $Ra = 10^9$ a time of $100T$ corresponds to about 1.7 h; in the experiment they found that this time is adequate for first-order statistics, like the Nusselt number, while more than 8 h were necessary in order to pin down the error bar of second-order statistics (P. Tong, personal communication). Du & Tong (2000), however, obtained their statistics from single-point measurements and they could only average their data in time; for the present numerical simulations, in contrast, simultaneous measurements over several points in homogeneous regions are

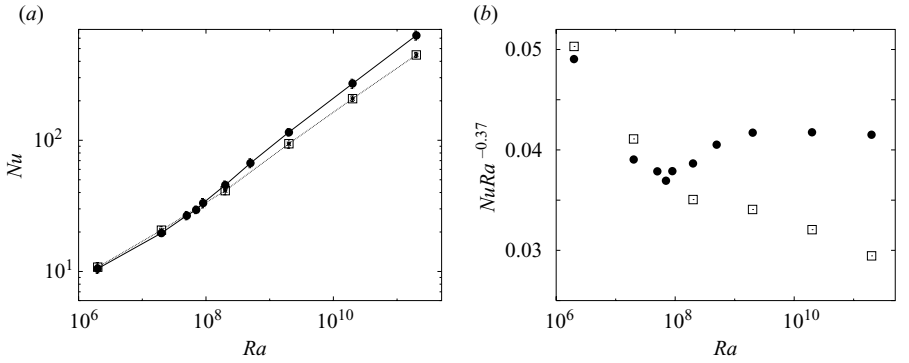

FIGURE 5. (*a*) Nusselt number as a function of the Rayleigh number for the three-dimensional cases at $Pr = 0.7$: □, smooth plates; ●, grooved plates. (*b*) The same as (*a*) for the Nusselt number compensated with $Ra^{-0.37}$. In (*a*) also the error bars are reported, they are, however, generally smaller than the symbol size. The results for smooth plates are from Verzicco & Camussi (2003).

carried out and the data averaging can be performed also among different probes. In particular, about 400 numerical probes as described in Verzicco & Camussi (2003) are placed within the computational domain, half of which are in the bulk of the flow and the remaining equally distributed between hot and cold boundary layers. The latter, in turn, are positioned over the tips and the throats of the grooves so that each type of measurement can benefit from the averaging of about 50 different probes.

3. Results

3.1. *Heat transfer measurements*

As mentioned in § 1, the most evident effect produced by the grooved plates is an increase of the heat transfer that in non-dimensional form is expressed by the Nusselt number. This is confirmed also by the present results (figure 5) showing that after a threshold Rayleigh number Ra_{th}, the heat transfer with the grooved plates increases with a steeper power law than the flat-plate counterpart. Since the computation of the Nusselt number with the grooved plates implies some non-trivial choices, a short discussion follows in order to clarify the meaning and the effects of the various variables. Integration of (2.1*c*) between the lower grooved plate and a generic section S at height z yields:

$$\int_{S_w} \nabla\theta \cdot \boldsymbol{n}\, \mathrm{d}S = \left(\sqrt{RaPr}\, \overline{u_z\theta} - \frac{\partial \overline{\theta}}{\partial z} \right)_z S, \tag{3.1}$$

where S_w is the wet surface of the grooved plate, $S = \pi d^2/4$ is the cross-sectional area of the cell and the operator $\overline{(\ )}$ implies an average over a constant height section. Since the left-hand side of equation (3.1) is the heating power Φ flowing from the lower plate into the fluid, the Nusselt number is given by the heat flux normalized by the cross-section S, namely $Nu = \Phi/S \equiv (\sqrt{RaPr}\, \overline{u_z\theta} - \partial\overline{\theta}/\partial z)_z$. Other quantities implied in the Nusselt number definition are implicitly included in the non-dimensional definition of (2.1*c*); these are in particular the total temperature difference Δ and the base-to-base distance between the plates h. It is worth mentioning that the use of the base-to-base height h follows the convention adopted by Du & Tong (2000) this, however, is only

one among several possibilities given by different heights. For example the tip-to-tip height would be $h_T = 0.95h$ and the volume-averaged height $h_V = V/S = 0.975h$ with $V = \pi d^2 h/4 - \sum_{i=1}^{5} 2\pi\delta^3(2i-1)$ the volume of fluid contained in the cell. It is easy to show that from $Nu = ARa^{\beta}$, $\mathrm{d}\beta/\beta = [(1-3\beta)/\ln Nu](\mathrm{d}h/h)$ results which in the low end of Ra gives at most $\mathrm{d}\beta/\beta = 0.15\,\%$ (with $Nu = 10$, $\beta = 2/7$ and $\mathrm{d}h/h = 0.05$) and in the high end of Ra $\mathrm{d}\beta/\beta = -0.36\,\%$ (with $Nu = 1000$, $\beta = 1/2$ and $\mathrm{d}h/h = 0.05$). On the other hand, Du & Tong (2000) have shown that $\mathrm{d}A/A = (1-3\beta)\,\mathrm{d}h/h$ is, at most, of the order of 1 % thus indicating that the corrections are clearly too small to be appreciated by any experimental or numerical measurement and that the particular definition of h is not a critical issue. As an aside, we note that if $\beta = 1/3$ then $\mathrm{d}\beta/\beta \equiv 0$ and $\mathrm{d}A/A \equiv 0$ implying that the relation $Nu = ARa^{\beta}$ is completely unaffected by h; this is the classical argument by Malkus (1954).

Another factor deserving a comment is that the wet surface of the plate is S_w while the Nusselt number is normalized by the cross-sectional area of the cylindrical cell S. Since for the present geometry it results in $S_w = \sum_{i=1}^{10} \sqrt{2}\pi\delta^2(2i-1) = \sqrt{2}S \simeq 1.41S$ it could be argued that the heat transfer enhancement is simply due to the increase of wet area. Should this be the case, the Nusselt number variation would be bounded by the increase of wet area and it would consist of an upward shift of the Nu versus Ra relation without any change in the power law exponent. In contrast, Du & Tong (2000) obtained a 76 % increase of heat transfer with an augmented wetted area of only 41 % while Roche *et al.* (2001) measured a $\beta = 0.51$ power law over one and half Ra-decades in a configuration that, using smooth plates, had a power law with $\beta = 0.39$.

For the present numerical simulations, the results are given in figure 5 where it is shown that the heat transfer with grooved plates initially is similar to that with smooth plates, but eventually follows a power law with an increased exponent ($Nu \sim Ra^{0.37}$). The crossing with the flat-plate data occurs at $Ra_{th} \simeq 4 \times 10^7$ that, computing an 'average' thermal boundary-layer thickness by the relation $\bar{\lambda}_\theta = h/(2Nu)$, yields $\bar{\lambda}_\theta/h \simeq 2.20 \times 10^{-2} \simeq \delta/h$; once more this confirms that the plate asperities enhance the heat transfer when they are not buried below the thermal boundary layer. In §§ 3.2 and 3.3, we will analyse the flow changes produced by the non-smooth plates and in § 4 these results will be discussed and compared with similar cases from the literature.

It should be stressed that the value $Ra_{th} \simeq 4 \times 10^7$ should be taken with caution since it was obtained by linearly connecting the points of the simulations and computing the crossing of the segments. On account of the error bars, it can be assumed that the crossover of the flows occurs in the range $2 \times 10^7 \leqslant Ra \leqslant 9 \times 10^7$, this, however, does not alter the previous conclusions.

It is worth mentioning that the results of figure 5 as well as all the other simulations performed in this study have been obtained at $Pr = 0.7$. The main reason for this choice is that in order to be able to distinguish the effects of the grooved plates in otherwise ideal conditions, we needed to compare the results against similar ideal flows with smooth plates. The papers by Verzicco & Camussi (2003) and Verzicco (2003) have in fact been obtained for flat plates in a cylindrical cell of aspect-ratio $\Gamma = 1/2$ at $Pr = 0.7$ for the same range of Rayleigh numbers and therefore are the best candidates for such a comparison. Of course this value of the Prandtl number is different from that of the experiments in water (Shen *et al.* 1996; Ciliberto & Laroche 1999; Du & Tong 2000) and this might cause differences in the flow dynamics. It has been observed, however, that many flow features and especially the Nusselt number become essentially independent of Pr when the latter exceeds a threshold of about

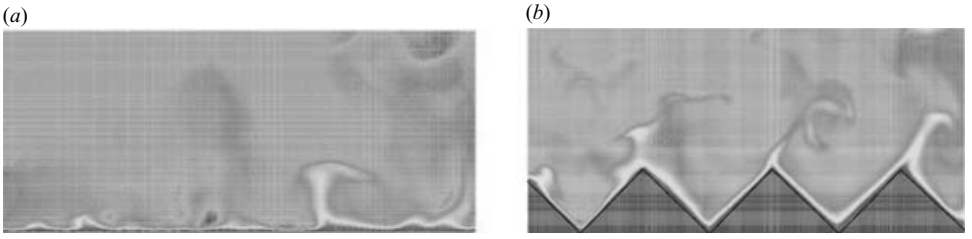

FIGURE 6. Instantaneous temperature field in a vertical section at $Pr = 0.7$ and $Ra = 2 \times 10^{10}$ (close-up of the hot boundary layer); (*a*) smooth plate, (*b*) grooved plate. The grey scale ranges from $\theta = 1$ (darkest grey) to $\theta = 0.35$.

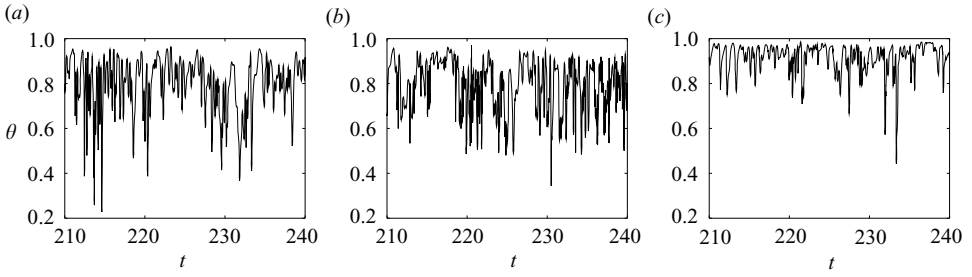

FIGURE 7. Time histories of temperature sampled inside the thermal boundary layer at a distance $z/h = \lambda_\theta/2$ from the hot surface, $Pr = 0.7$ and $Ra = 2 \times 10^{10}$. (*a*) smooth plate, (*b*) tip of the grooved plate, (*c*) throat of the grooved plate.

0.35 (Verzicco & Camussi 1999) thus making possible the comparison of the present simulations with the experiments in water.

3.2. *Near-wall dynamics*

As shown in the paper by Du & Tong (2000), the presence of asperities on the plate surface dramatically changes the plume emission and therefore the heat transfer. Their findings can be summarized by figure 6 showing typical plume emissions from smooth and grooved plates. In the first case, the plume eruption is a purely buoyancy-driven phenomenon while in the second, the presence of grooves favours the flow separation at the sharp edges thus enhancing the plume generation and fixing in space the location of the emission. The described behaviour is shown in figure 7 where representative time series at a fixed distance from the wall $z/h = \lambda_\theta/2$ are reported for the flat and the grooved plates; in the latter case, the signals are separately sampled over the tips and in the throats in order to stress the different dynamics. The cold spikes in the signals indicate the plume shedding since they evidence the 'cold' fluid from the bulk sweeping the hot plate and replacing the thermal plumes that have been released immediately before. It can be seen that in the case of the smooth plate, the plumes are released less frequently than over the tips of the grooved plate. In the throat, in contrast, the fluid is basically stagnant and the signal is characterized by a higher mean temperature and a reduced fluctuation level. Occasionally, however, large intense events occur and they are the intermittent rising of bubbles of hot fluid that have gained enough heat after a long residence time in the throat. While the signals of figure 7 represent only a small time window of the whole simulation and only for a single-point measurement, the collective near-wall behaviour can be appreciated from figure 8 which includes all the probes placed

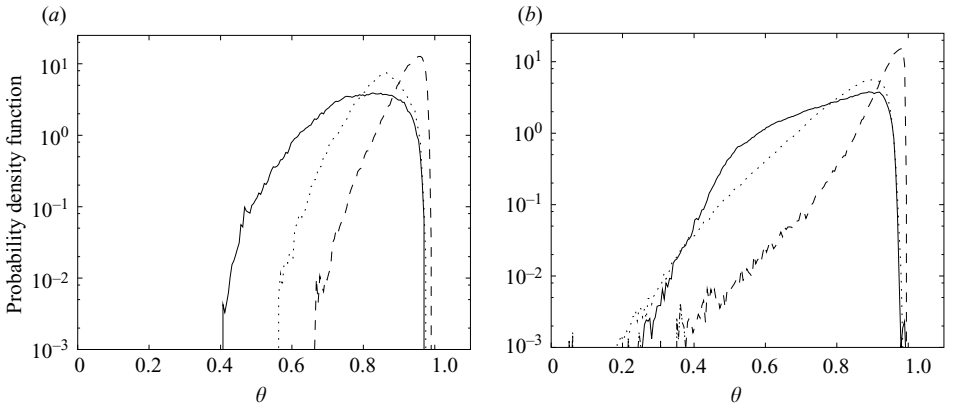

FIGURE 8. Probability density functions of temperature inside the hot plate temperature boundary layer: ···, smooth wall; ———, tip of the grooved plate; ----, throat of the grooved plate. (*a*) $Pr = 0.7$ and $Ra = 2 \times 10^7$, (*b*) $Pr = 0.7$ and $Ra = 2 \times 10^{10}$.

within the thermal boundary layer (about 50) and for the whole duration of the computations. The presence of large tails on the left evidences the cold fluid from the bulk replacing the shed plume while their increased probability indicates the enhanced shedding frequency. The mean x-value of the histograms yields the mean temperature of the point that, given the fixed wall temperature and distance of the probes from the surface, indicates also the local heat transfer. The described features are present before and after the transitional Rayleigh number, although in the latter case they are more pronounced. In particular, at $Ra = 2 \times 10^7$, mean and r.m.s. temperature are, respectively, $\overline{\theta} = 0.850$ and $\sigma = 0.060$ for the flat plate while they result in $\overline{\theta} = 0.931$ and $\sigma = 0.041$ in the throat of the groove and $\overline{\theta} = 0.792$ and $\sigma = 0.097$ over the tip. At $Ra = 2 \times 10^{10}$, the same quantities assume the values $\overline{\theta} = 0.832$ and $\sigma = 0.098$ for the flat plate, $\overline{\theta} = 0.946$ and $\sigma = 0.051$ in the throat and $\overline{\theta} = 0.784$ and $\sigma = 0.122$ over the tip. Apart from the different values, however, the most distinctive feature of the flow before and after Ra_{th} is the frequency of the plume shedding over the tips that, in the latter case, is strongly enhanced.

It is worth mentioning that similar features have been observed also by Du & Tong (2000) that, however, had to account for the non-uniform temperature of the plates owing to the finite (although high) thermal conductivity of the plate material (brass). Talking about the upper cold plate they say: 'Unlike the smooth surface, the rough surface is no longer isothermal under uniform heating. . . . This non–uniform boundary layer dynamics destroys the surface homogeneity and produces a higher surface temperature at the tip.' Another important factor is that the used thermistor had a core with a diameter of 0.29 mm with a layer of glass coating of 0.1 mm thickness therefore the local temperature measurement were strongly influenced by the mean temperature inside the boundary layer (P. Tong personal communication). Despite these differences, the near-wall dynamics is captured well by the measurements of Du & Tong (2000) and the agreement with the present results is remarkable.

The altered boundary-layer dynamics is another distinctive feature of the grooved plates and some of the details for the mean and r.m.s. temperature vertical profiles are given in figures 9 and 10. As could be argued already from the previous discussion, the wall temperature gradient, and therefore the local heat transfer, is the most intense at the tips while it attains the minimum value in the throats. Here the profiles

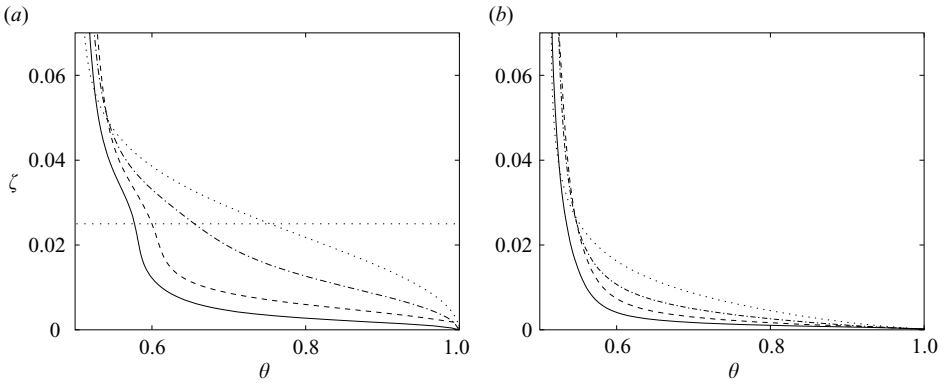

FIGURE 9. Vertical profiles of mean temperature for the lower hot grooved plate at $Pr = 0.7$: ——, $Ra = 2 \times 10^{10}$; - - - -, $Ra = 2 \times 10^{9}$; –·–, $Ra = 2 \times 10^{8}$; · · ·, $Ra = 2 \times 10^{7}$. (*a*) profiles in the throats, (*b*) profiles over the tips. ζ is the vertical distance from the solid surface, the horizontal/dotted line is the maximum height of the grooves.

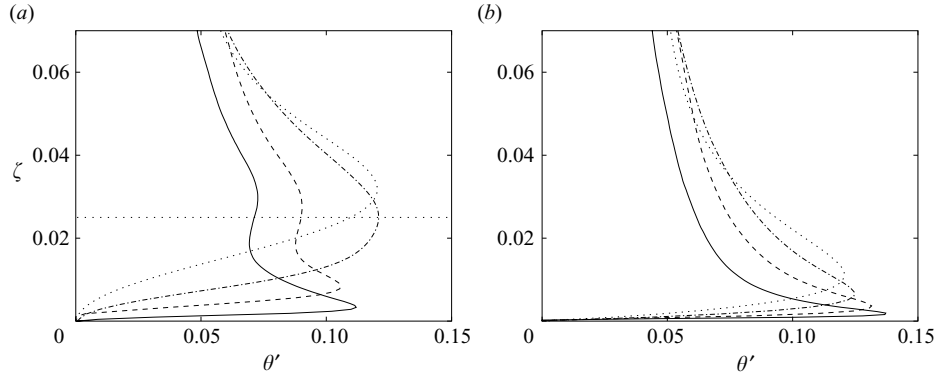

FIGURE 10. Vertical profiles of r.m.s. temperature fluctuations for the lower hot grooved plate at $Pr = 0.7$: ——, $Ra = 2 \times 10^{10}$; - - - -, $Ra = 2 \times 10^{9}$; –·–, $Ra = 2 \times 10^{8}$; · · ·, $Ra = 2 \times 10^{7}$. (*a*) profiles in the throats, (*b*) profiles over the tips. ζ is the vertical distance from the solid surface, the horizontal dotted line is the maximum height of the grooves.

show a change of shape when the Rayleigh number crosses the transitional value; this is particularly evident from the r.m.s. profiles of figure 10(*a*) showing that when the main r.m.s. peak goes below the groove height δ, a secondary peak develops at $z = \delta$ and this is produced by the unsteady interaction between the secondary recirculation inside the groove and the external mean wind (figure 11). Assuming the position of the r.m.s. temperature peak as the thickness of the thermal boundary layer, it is possible to draw the thickness distribution over a groove as shown in figure 12. The profiles have been averaged in the azimuthal direction, in time and over the 5 grooves in order to obtain a single representative thickness distribution for each Rayleigh number. As already argued in several papers, only when the mean thermal boundary-layer thickness, estimated as $\overline{\lambda}_\theta = h/(2Nu)$, becomes smaller than the groove height δ the heat flux is enhanced with respect to the flat-plate case. It is also significant that when the same thickness (namely, that obtained by the position of the r.m.s. temperature peak) is distributed over the groove, it coincides for most of the surface with the local thermal boundary-layer thickness λ_θ computed

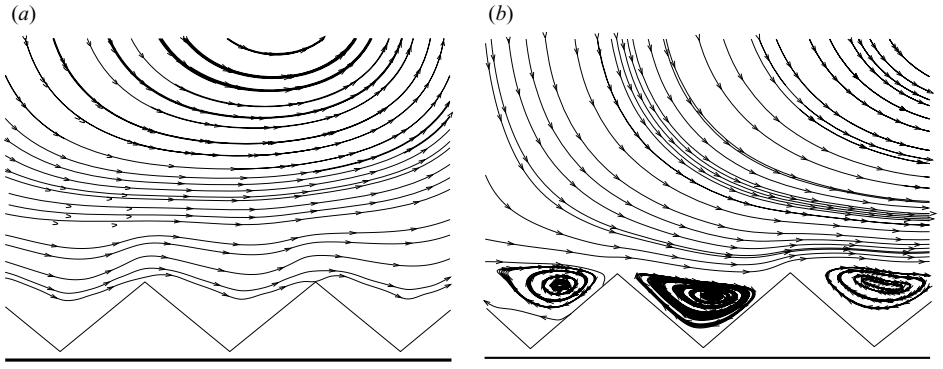

FIGURE 11. Streamlines on a vertical section to evidence the secondary recirculations inside the grooves (closeup of the lower hot grooved plate); (*a*) $Ra = 2 \times 10^7$, (*b*) $Ra = 2 \times 10^{10}$.

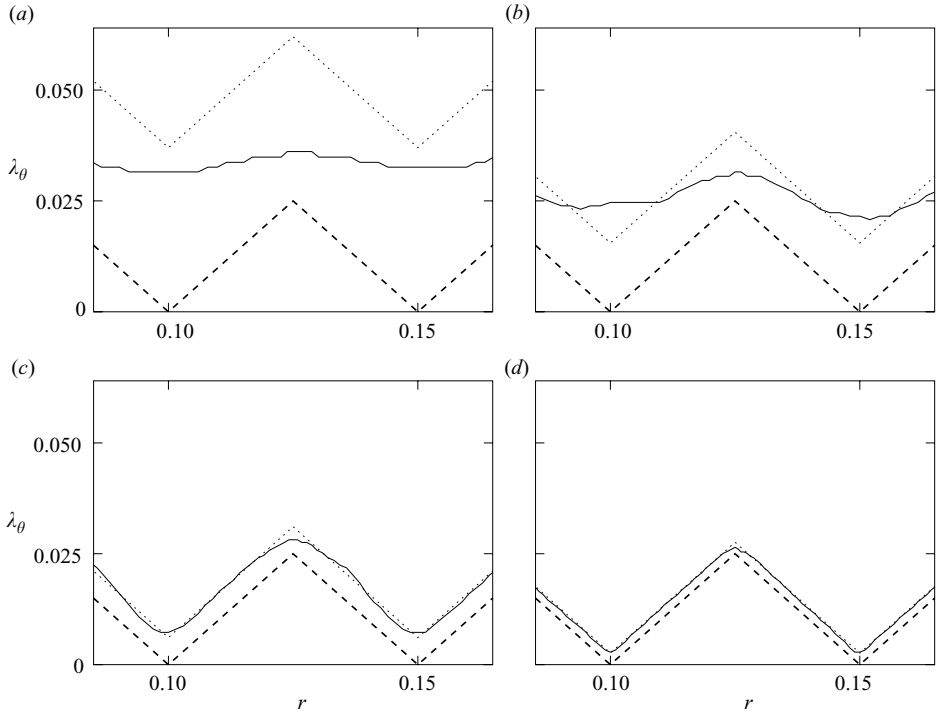

FIGURE 12. Radial profiles of a 'typical' groove of the thermal boundary-layer thickness at $Pr = 0.7$: (*a*) $Ra = 2 \times 10^7$, (*b*) $Ra = 2 \times 10^8$, (*c*) $Ra = 2 \times 10^9$ and (*d*) $Ra = 2 \times 10^{10}$. ----, geometry of the groove; ——, thermal boundary-layer thickness; $\cdots$, line at a constant distance $h/(2Nu)$ from the groove surface with Nu taken from figure 5.

as the position of the r.m.s. temperature fluctuation peak; this implies that despite the different flow dynamics, the heat transfer is quite uniform over the groove surface suggesting that the plumes released from the tips essentially collect the fluid heated along the sides of the grooves. As an aside we note that, since both the Nusselt number and the boundary-layer thickness are computed from the same data but over different quantities, the coincidence of $\overline{\lambda}_\theta$ with the factor $h/(2Nu)$ can be regarded as a cross-validation for the computation of the Nusselt number.

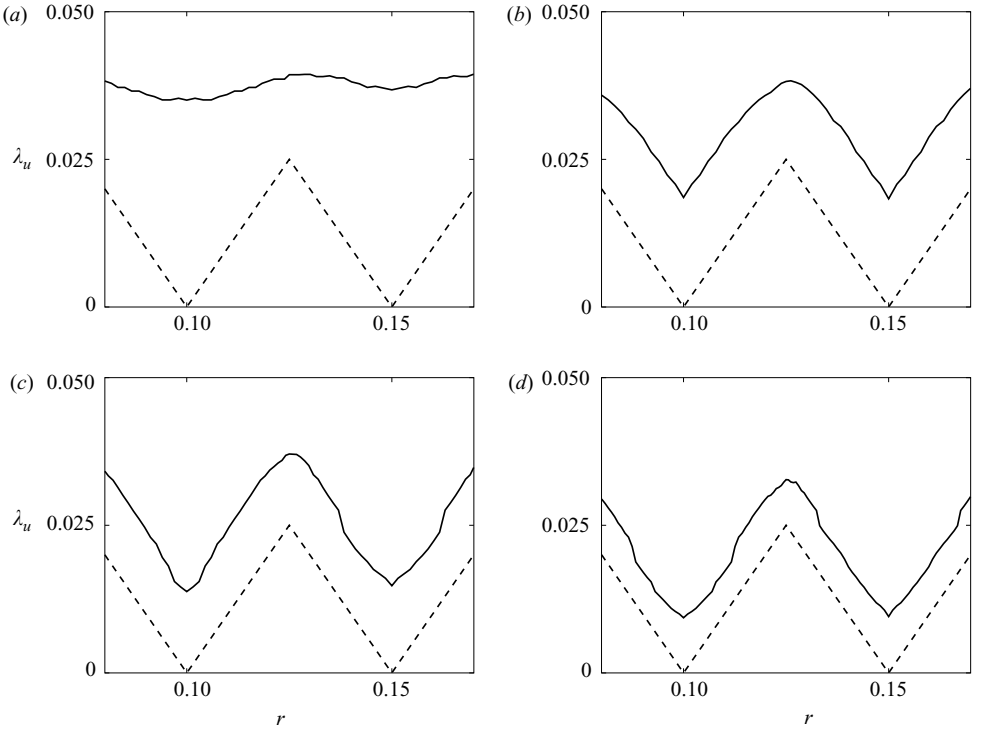

FIGURE 13. Radial profile of a 'typical' groove of the viscous boundary layer thickness at $Pr = 0.7$: (*a*) $Ra = 2 \times 10^7$, (*b*) $Ra = 2 \times 10^8$, (*c*) $Ra = 2 \times 10^9$ and (*d*) $Ra = 2 \times 10^{10}$. ----, geometry of the groove, ——, viscous boundary layer thickness.

The fact that according to figure 12 the thermal boundary-layer thickness is constant over the groove surface seems to contradict the idea that the plumes are released mainly from the tips of the grooves. However, since it results in $\lambda_\theta < \lambda_v$, the heat transfer on the sides of the groove is essentially diffusive while convection only occurs at the tip where temperature and vertical velocity fluctuations are correlated.

It is worth mentioning that the local thermal boundary-layer thickness has been computed as the distance from the wall of the r.m.s. temperature peak in the vertical direction while the heat transfer is proportional to the wall normal temperature gradient. Since the wall normal is always at an angle of $\phi = \pi/4$ with respect to the vertical direction, the local specific heat transfer can be estimated as $\kappa(\Delta/2)/(\lambda_\theta \cos\phi)$ where κ is the thermal conductivity of the fluid and the factor $\Delta/2$ is due to the fact that only half of the total temperature difference Δ is supported by each thermal boundary layer. On the other hand, the wet area of the plate is $S_w = S/\cos\phi$ therefore the surface-averaged heat transfer normalized by the purely conductive value $(\kappa \Delta S/h)$, or in other words the Nusselt number, yields again the relation $\overline{\lambda}_\theta/h = 1/(2Nu)$ which is confirmed from the results of figure 12.

The viscous boundary layers, computed from the peak position of the r.m.s. profiles for the velocity component parallel to the conducting wall, are shown in figure 13 and they behave similarly to the thermal ones with the only relevant difference that they thicken around the tips instead of becoming thinner. The reason is that the velocity parallel to the wall also contains a vertical component that is reinforced by the plume emission. In other words, the tips of the grooves anchor the vertical jets formed by the

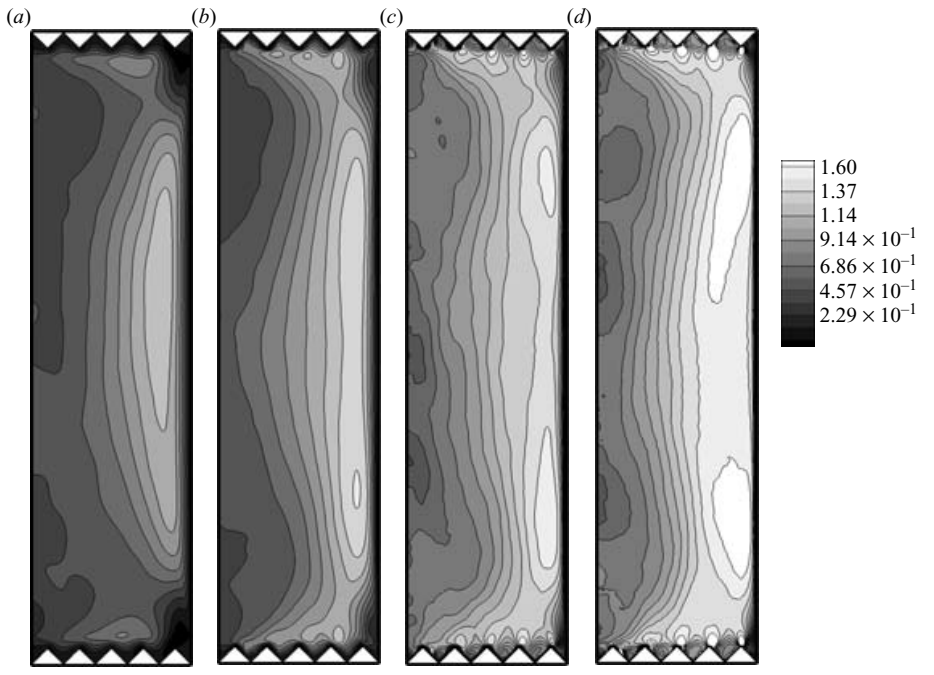

FIGURE 14. Maps of the correlation $\langle u_z'\theta' \rangle$ averaged in time and in the azimuthal direction. (*a*) $Ra = 2 \times 10^7$, (*b*) $Ra = 2 \times 10^8$, (*c*) $Ra = 2 \times 10^9$, (*d*) $Ra = 2 \times 10^{10}$. In order to maintain the same range at different Rayleigh numbers the correlation has been normalized according to the following expression $\sqrt{RaPr}\,\langle \theta' u_z' \rangle / Nu$.

sequence of emitted plumes. The flow here has a strong vertical unsteadiness which produces intense velocity fluctuations, in turn thickening the viscous boundary layer. Of course, the discussed phenomenon can occur only if thermal plumes are effectively emitted from the tips, which implies $Ra > Ra_{th}$. For smaller Rayleigh numbers, the grooves lie just inside the boundary layers, producing negligible effects in the near-wall (figure 13*a*) and external flow (figure 11*a*).

Further evidence of the altered boundary-layer dynamics is stressed by the r.m.s. peaks of figure 10(*b*) whose value increases monotonically with *Ra*. This behaviour is different from the smooth plate (Verzicco & Camussi 2003) where the r.m.s. temperature peak remains constant with a Rayleigh number at least up to $Ra \approx 10^{12}$ where a laminar/turbulent boundary-layer transition seems to occur (Chavanne *et al.* 1997; Niemela & Sreenivasan 2003). The altered level of temperature fluctuations at the groove tip, combined with the geometrically induced flow separation, enhances the correlation $\langle \theta' u_z' \rangle$ which is the convective heat transfer. Figure 14 shows the maps of this correlation for different Rayleigh numbers. Following the definition of the Nusselt number of equation (3.1) the correlations are normalized according to $\sqrt{RaPr} < \theta' u_z' > / Nu$ so that the flows at different Rayleigh numbers can be compared within the same range of values. We have preferred this normalization with respect to the more classical $\langle \theta' u_z' \rangle / (\langle \theta' \rangle \langle u_z' \rangle)$ because the latter would range between 0 and 1 for every Rayleigh number and would not allow us to appreciate the relative contribution to *Nu* of the correlation $\langle \theta' u_z' \rangle$ as a function of *Ra*. Figure 14 confirms that for $Ra < Ra_{th}$, the surface grooves lie below the thermal boundary layer and the stagnant fluid inside the grooves partially insulates the large-scale recirculation from

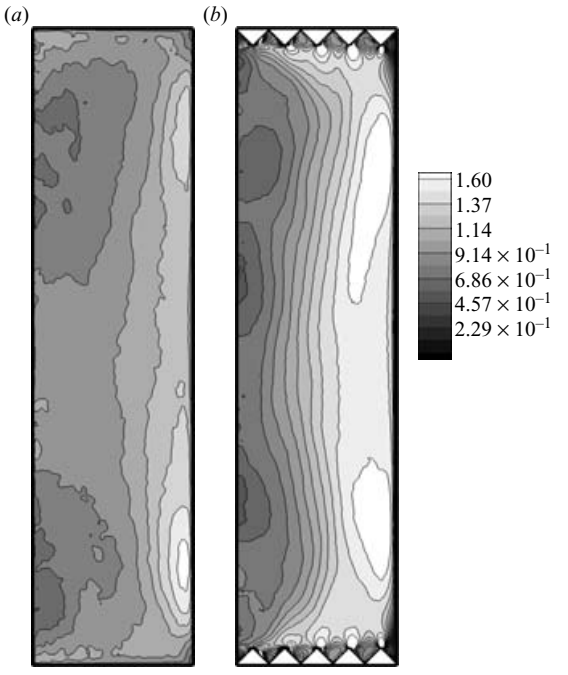

FIGURE 15. The same as figure 14 at $Ra = 2 \times 10^{10}$: (*a*) flow with smooth plates, (*b*) flow with grooved plates.

the heated (or cooled) surface (figure 11*a*); this effect makes up for the increased wet area and the resulting Nusselt number assumes a value approximately equal to that of the smooth plate. In contrast, when $Ra > Ra_{th}$, the thermal boundary layer is thin enough for the grooves to protrude into the large-scale flow; in this case, the interaction of the secondary recirculations with the mean wind (figure 11*b*) contributes to the total heat transport while the additional activity over the tips determines the extra heat flux.

The positive effect of the grooves on the heat transfer is particularly evident from figure 15 where a comparison at the same Ra with the smooth-plate case is performed. Since the large-scale flow sweeps the plates via the mean wind, the plumes released from the smooth surface are initially dragged horizontally and only eventually in the vertical direction when the mean current is bent to follow the sidewall. The convective heat transfer, however, is sensitive only to the vertical velocity and therefore it is relevant only in the second phase when part of the heat carried by the plumes is already lost to the ambient fluid by diffusion; this scenario is very close to that proposed by Kadanoff (2001) in his famous cartoon. On the other hand, the presence of grooves allows the direct injection of the plumes in the vertical direction, which therefore contribute, from their generation, to the convective heat transport. In other words, in addition to enhancing the plume generation, the grooves increase their vertical penetration into the mean flow thus augmenting the heat flux. This is better understood when considering that, owing to impermeability, the vertical velocity of a plume released from a flat plate initially can only increase as the square of the wall distance, whereas from a grooved plate, this restriction does not apply because the wall-normal direction is not vertical. This effect is presumably maximized when the large-scale recirculation is absent since the plume released vertically keeps rising owing

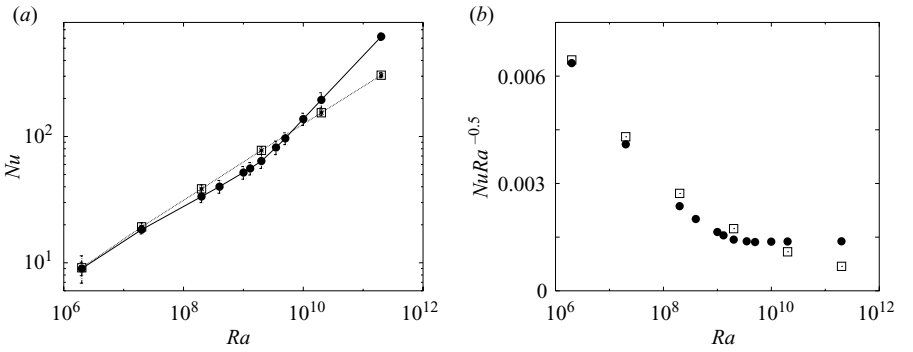

FIGURE 16. (*a*) The Nusselt number as a function of the Rayleigh number for the axisymmetric flows at $Pr = 0.7$: □, smooth plates; ●, grooved plates. (*b*) The same as (*a*) for the Nusselt number compensated with $Ra^{-0.5}$. The data for the flat plates are from Verzicco (2003).

to buoyancy, without any deviation. This might be the case for the axisymmetric flow when a single large recirculation completely filling the cell obviously cannot develop (Verzicco 2003); within this scenario the Nusselt number of figure 16 that in the presence of grooves increases faster than the three-dimensional flow, is consistent with the proposed argument. In addition we note that the *Nu vs. Ra* relation eventually attains the 1/2 power law which was observed by Roche *et al.* (2001) for a similar groove geometry (although distributed also on the sidewall), but within a higher Rayleigh-number range ($10^{12} \leqslant Ra \leqslant 5 \times 10^{13}$). According to Stringano & Verzicco (2006) in this range of Rayleigh numbers, and for a $\Gamma = 1/2$ cylindrical cell, the mean flow should be absent or at least strongly weakened and the initial plume dynamics might have similarities with the axisymmetric flow. This consideration, however, is only speculative and deserves further investigation since at high Rayleigh numbers, the boundary layers are known to undergo a transition from a laminar to a turbulent regime (Chavanne *et al.* 1997; Niemela & Sreenivasan 2003) which clearly cannot occur in an axisymmetric flow.

3.3. *Bulk dynamics*

The flow dynamics in the bulk essentially agrees with the description of Du & Tong (2001) who report an increased level of fluctuations due to the enhanced plume emission from the grooved plates. This is confirmed by the probability density function of temperature and vertical velocity shown in figure 17. In particular, before the transition ($Ra < Ra_{th}$) neither the shape nor the fluctuation level is affected by the plate grooves while, in contrast, for $Ra > Ra_{th}$ the probability density functions preserve their shape although the fluctuations increase in magnitude. This is confirmed by figure 18 showing the collapse onto a unique curve when each p.d.f. is rescaled by its r.m.s. value. The dependence of the r.m.s. fluctuations on the Rayleigh number is shown in figure 19 for velocity and temperature and in both cases it is observed that they increase only when $Ra > Ra_{th}$. This is consistent with the scenario proposed in § 3.2 with the grooved plates insulated by a layer of stagnant fluid before the transition and the tips enhancing the frequency of the plume shedding for $Ra > Ra_{th}$.

Similar indications are given by the spectra of figure 20 which show the same slopes and shapes at every Rayleigh number except for the augmented fluctuation

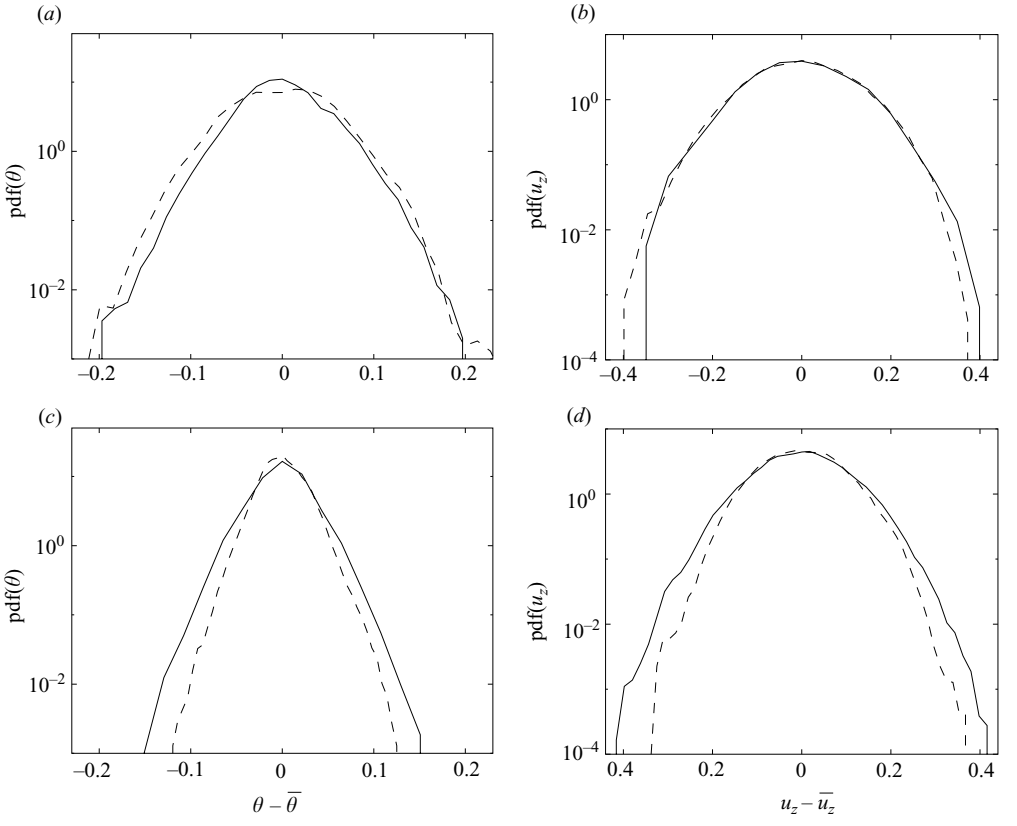

FIGURE 17. Probability density functions of (a, c) temperature and (b, d) vertical velocity in the bulk of the flow. ———, grooved plates; - - - -, smooth plates. (a, b) $Ra = 2 \times 10^7$, (c, d) $Ra = 2 \times 10^{10}$.

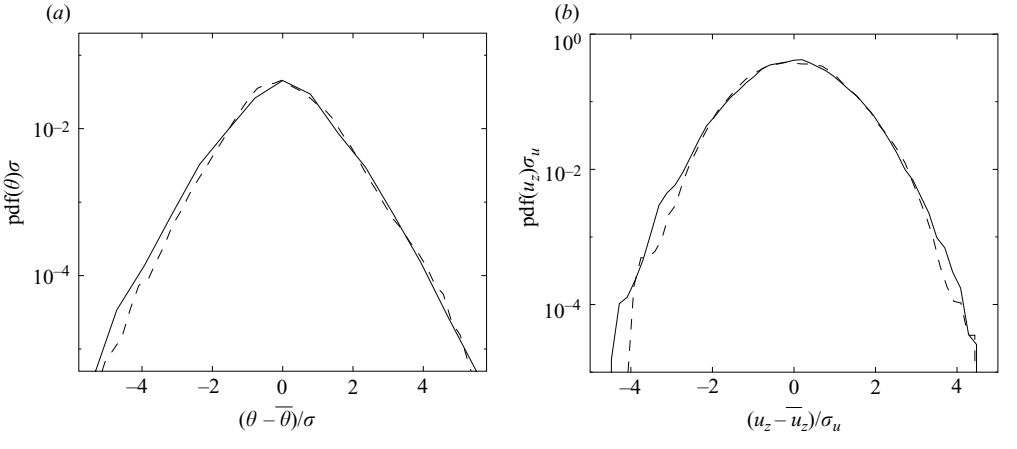

FIGURE 18. Probability density functions normalized by the r.m.s. of (a) temperature and (b) vertical velocity at $Ra = 2 \times 10^{10}$ in the bulk of the flow. ———, grooved plates; - - - -, smooth plates.

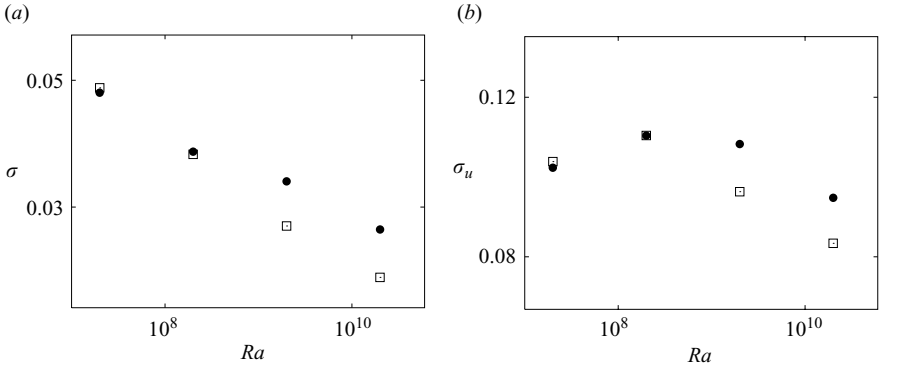

FIGURE 19. Root mean square of (a) temperature and (b) vertical velocity as function of Ra in the bulk of the flow. □, grooved plates; ●, smooth plates.

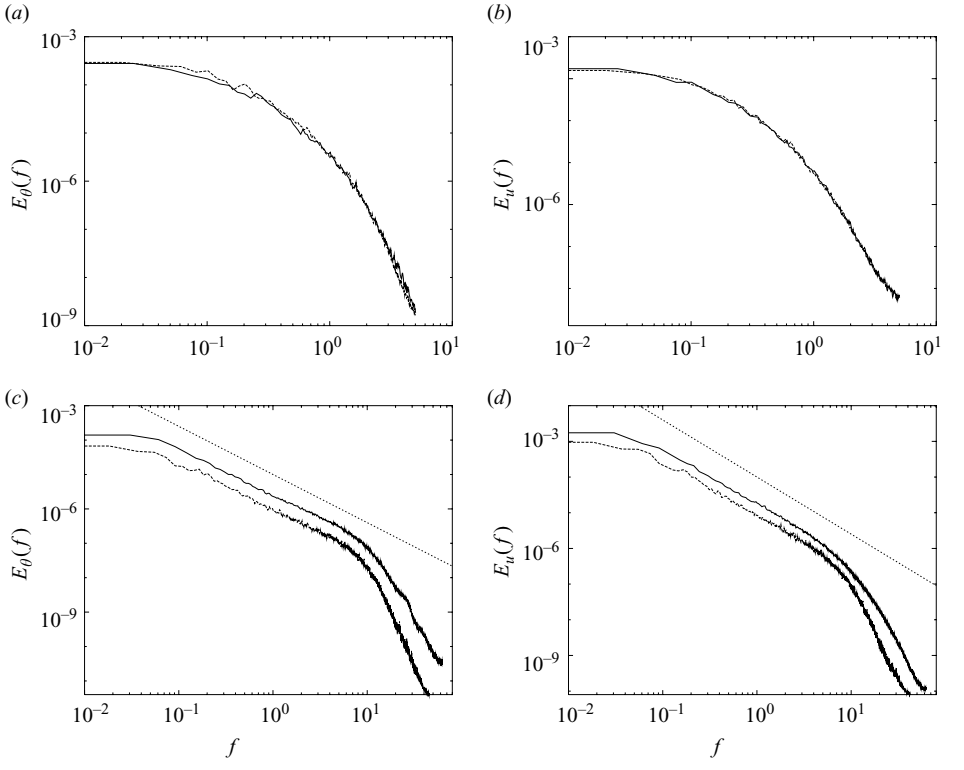

FIGURE 20. Spectra of (a, c) temperature and (b, d) vertical velocity in the bulk of the flow. ——, grooved plates; - - - -, smooth plates. (a, b) $Ra = 2 \times 10^7$, (c, d) $Ra = 2 \times 10^{10}$. The straight line in (c) is the slope $-7/5$, while in (d) it is $-5/3$.

level beyond the transition. It is worth mentioning that, as noted by Verzicco & Camussi (2003) and Camussi & Verzicco (2004), the slope of the inertial part of the temperature spectra is $-7/5$ while that of the velocity is $-5/3$; is seems, therefore, that the temperature follows the Bolgiano dynamics while the velocity evolves according to the standard Kolmogorov scenario. This apparent contradiction is solved when considering that the Bolgiano dynamics emerges only when the Bolgiano length L_B is smaller than the integral scale L_i (respectively, L_u and L_θ for velocity

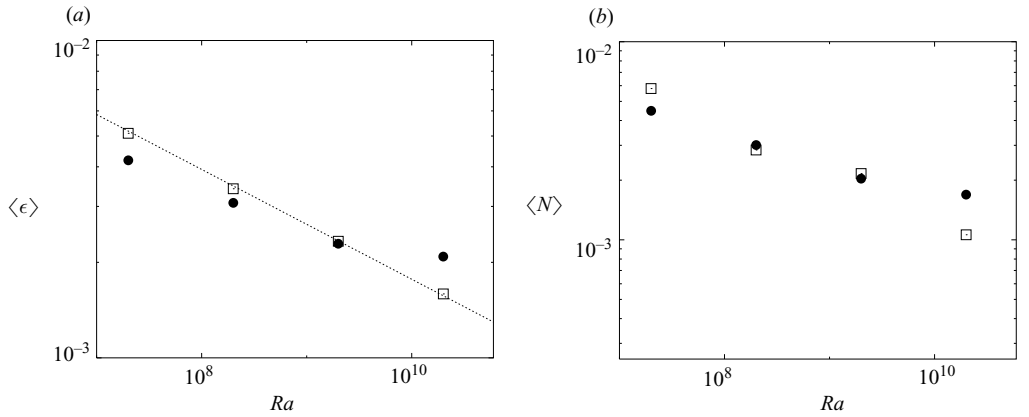

FIGURE 21. (*a*) Kinetic energy and (*b*) temperature variance dissipation rates as a function of the Rayleigh number. □, smooth plates; ●, grooved plates. The dotted line in (*a*) is the slope $\beta - 1/2 \simeq -0.2$ with β computed from the smooth-plate data of figure 5.

and temperature fields) and only within the range of scales $L_i \geqslant \ell \geqslant L_B$. Verzicco & Camussi (2003) and Camussi & Verzicco (2004) have shown, by direct computation of the quantities from the three-dimensional data fields, that for the present problem it results in $L_B < L_\theta$ and $L_B > L_u$ thus justifying the different scalings of the spectra. The difference between L_θ and L_u can be intuitively understood considering that the integral scale is the length at which the forcing occurs. In the Rayleigh–Bénard problem, the horizontal plates are kept at different temperatures, therefore, the temperature forcing occurs at a scale of the order of their distance $L_\theta \approx h$ which is the largest in the flow. In contrast, the forcing of the velocity field depends on the structure of the mean flow and its dynamics which are both Ra dependent. Another intuitive interpretation was given by Grossmann & Lohse (1991) who suggested that the main effect of the temperature is to put potential energy into the generation of a large-scale mean flow, the kinetic energy of which cascades down to the smaller scales according to the classical Richardson and Kolmogorov mechanism. On the other hand, the temperature fluctuations still drive vertical velocity fluctuations and this makes the temperature an active scalar that therefore undergoes the Bolgiano dynamics.

As already mentioned, for $Ra > Ra_{th}$, the effect of the grooves is to increase the energy of the fluctuations at all scales which shown in figure 20 results in an upward shift of the spectra; this, however, implies also an increase of the dissipation which is shown more clearly by a shift to the right of the dissipative range of the same spectra. This point is in figure 21 where both temperature variance and kinetic energy dissipation rates, respectively, $\langle N\rangle$ and $\langle\epsilon\rangle$, are computed from the spatial gradients of the three-dimensional temperature and velocity fields. In more detail, given the non-dimensional form of the equations (2.1) it follows from the definitions $\langle\epsilon\rangle = \langle|\boldsymbol{\nabla u}|^2\rangle\sqrt{Pr/Ra}$ and $\langle N\rangle = \langle|\nabla\theta|^2\rangle/\sqrt{RaPr}$ where the operator $\langle\ldots\rangle$ implies averages over the fluid volume and in time. Figure 21 shows that before the transition, both $\langle N\rangle$ and $\langle\epsilon\rangle$ assume similar values for the smooth and the grooved plates, but for $Ra > Ra_{th}$, the dissipations for the grooved plates are always the largest. This result seems to disagree with Du & Tong (2001) who computed some quantities related to the dissipations and they found them to follow a unique law for the smooth and rough plates. It must be noted, however, that the results by Du & Tong (2001)

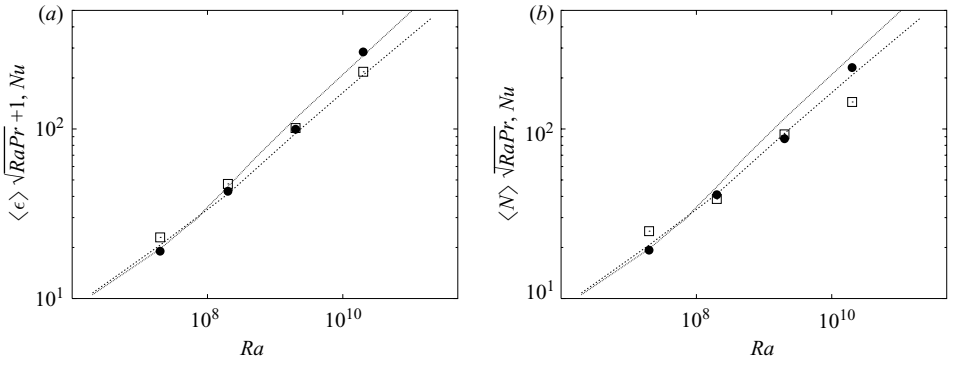

FIGURE 22. Normalized (*a*) kinetic energy and (*b*) temperature variance dissipation rates as functions of the Rayleigh number. □, smooth plates; ●, grooved plates. ——, the *Nu vs. Ra* relations for grooved and ···, for smooth plates of figure 5.

were obtained from single-point measurements in the bulk and therefore they cannot be taken as representative for the whole cell. In fact, Verzicco & Camussi (2003) have shown that most of the temperature variance dissipation rate $\langle N\rangle$ is within the wall region while the bulk contribution becomes negligible as the Rayleigh number increases.

As an aside we note that $\langle N\rangle$ and $\langle\epsilon\rangle$ are related to the Nusselt number by rigorous relations that in the present non-dimensional form read $\langle N\rangle = Nu/\sqrt{RaPr}$ and $\langle\epsilon\rangle = (Nu-1)/\sqrt{RaPr}$; this suggests that different values for the dissipations imply different values also for the Nusselt number which is what is obtained in figure 5. In particular, assuming $Nu \sim Ra^{\beta}$ it follows that $\langle N\rangle \sim Ra^{\beta-1/2}$ and $\langle\epsilon\rangle \sim Ra^{\beta-1/2}$ (the latter for $Nu \gg 1$). The slope in figure 21(*a*) is given by the power law $Ra^{\beta-1/2}$ with β computed from the smooth-plate data of figure 5. Since the dissipation for the grooved case decreases less rapidly with Ra, we can conclude that β increases for the grooved plates when $Ra > Ra_{th}$ which is a further confirmation of the results of figure 5.

Similar conclusions come from figure 21(*b*), even if the decrease of $\langle N\rangle$ is slightly too steep with respect to the power law $Ra^{\beta-1/2}$; although the reason for this discrepancy was not found, we can argue that it is due to difficulties in the computation of $\langle N\rangle$ at the boundaries, especially for the grooved case when the plate surface does not lie along a coordinate surface. This is confirmed by figure 22 where $\langle N\rangle$ and $\langle\epsilon\rangle$ are rescaled in such a way as to give the Nusselt number; although the agreement for $\langle\epsilon\rangle$ is better than for $\langle N\rangle$ in both cases, the results are consistent with the above arguments. We wish to stress, however, that this problem pertains only to the post-processed quantity $\langle N\rangle$ and it does not affect the flow computation which never requires $\langle N\rangle$ during the simulation of the flow dynamics.

4. Discussion and conclusions

In this paper, we have presented direct numerical simulations of three-dimensional confined thermal convection in the presence of grooved plates. In agreement with analogous experimental studies, it has been found that the heat transfer is enhanced when the mean thermal boundary-layer thickness $\overline{\lambda}_\theta$ becomes smaller than the roughness height δ and this condition yields a threshold Rayleigh number Ra_{th} which must be exceeded if the use of grooved plates is to be advantageous for the

heat transfer. In particular, it was shown that if the heat transfer is expressed through $Nu = ARa^{\beta}$, the grooved plates produce an increase of the exponent up to $\beta \approx 0.37$ to be compared with the value $\beta \approx 0.31$ of the flat plates. Indeed, in Verzicco & Camussi (2003), it was shown that for the smooth plates, the exponent β is $\approx 2/7$ for $Ra < 10^9$ and $\beta \approx 1/3$ for $Ra > 10^9$; the value $\beta \approx 0.31$ therefore should be considered only an average slope in the range $2 \times 10^7 \leqslant Ra \leqslant 2 \times 10^{11}$ investigated in the present paper.

It has been shown that the reason for the Nusselt number increase is the enhancement of plume emission from the tips of the grooves which strongly increases the correlation $\langle \theta' u_z' \rangle$, or in other words the convective heat transfer, already in the immediate vicinity of the plates. This is different from the flat-plate case where, in the same region, the heat transfer is mainly a diffusive phenomenon (see figure 15). This implies that the increase of the Nusselt number is not a trivial effect due to the increase of wet area, but rather to a complete change of the near-wall dynamics. As an aside, we note that increasing the contact area between a solid and a fluid is already a common practice in industry where finned surfaces are employed for the cooling of mechanical and electronic components.

Despite the different geometry of the rough elements and the experimental difficulties of Du & Tong (2000, 2001), the present results are in remarkable agreement with their findings especially for what concerns the near-wall dynamics and the mechanism for the enhancement of the plume formation.

The reason for the increased emission of plumes from the tips of the grooves can be easily understood by making an analogy of the static thermal problem with an electrical one. In particular, if the temperature difference $\Delta\theta$ is in analogy with the potential difference ΔV, the local heat flux ϕ with the current density I and the thermal conductivity of the fluid κ with the inverse of the electrical resistivity of the medium σ, the emission of a thermal plume is analogous to a 'spark' (because the heat field is analogous to the electric field). The analogy, however, remains valid only up to the point where the spark is released because immediately after, the medium crossed by the spark is ionized and this does not have any thermal analogue. Since in the present paper the grooved plates have been considered as perfectly conducting, their surface temperature is strictly constant. For an electrically superconducting material, this would imply that the surface potential is strictly constant and the potential field (figure 23*a*) is easily obtained by solving $\nabla^2 V = 0$ in the domain of interest. It is then evident that the maximum potential gradient (or the electric field) is over the tip which becomes the preferred location for the generation of a spark. This is the well-known 'wedge effect' which is the principle underlying the functioning of the lightning rods. If now we think of the equipotential lines of figure 23(*a*) as isothermal lines it is clear that the maximum temperature gradient is over the tip and this forces the strongest local heat flux (the plume formation) to occur in the same place. (It should be stressed that the analogy is not complete since the equation for the potential is $\nabla^2 V = 0$ while that for the temperature field is $\partial\theta/\partial t + \boldsymbol{u} \cdot \nabla\theta = k\nabla^2\theta$. However, in the immediate vicinity of the tip, with the surface temperature strictly constant also in time we can assume that the unsteady term is negligible. In addition, as shown in figure 13, the viscous boundary layer thickens around the tip which allows us to assume $\boldsymbol{u} \approx 0$; in this context, the two equations assume the same form. The same extension, however, is not correct for the whole domain of figure 23 since we have previously shown that in the presence of wedges, the convective heat transport is enhanced, suggesting that the presence of a nonlinear term would amplify the described effects and make the thermal depletion problem of figure 23(*b*) even more severe.)

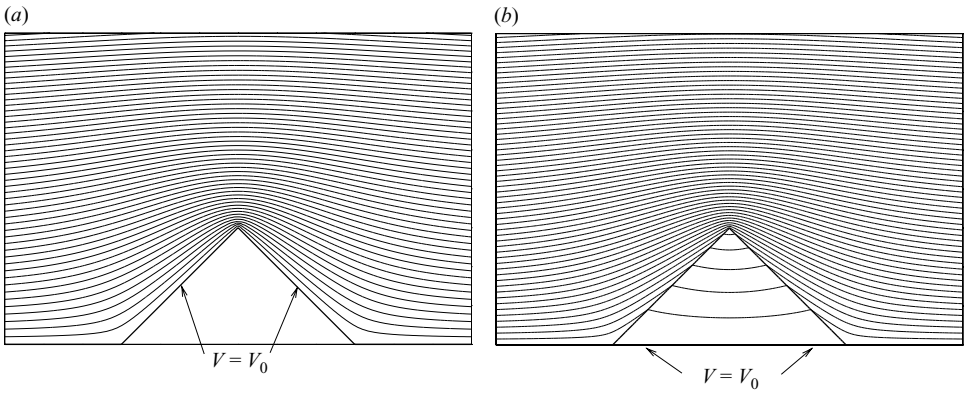

FIGURE 23. Isopotential lines over a two-dimensional wedge for (*a*) zero electrical resistance of the wedge, (*b*) electrical resistance of the wedge ten times smaller than that of the outer medium. Both problems have been solved for the steady state, imposing a total potential difference $\Delta V = 10$ between the lower and upper boundary (the latter outside of the figure) and with zero normal derivatives on the lateral walls.

The phenomenology is similar in the case of a wedge with a finite (although small) electrical resistivity which is analogous to a grooved plate with a finite (although large) thermal conductivity. In figure 23(*b*) it is observed, however, that the interface between the two media is no longer an equipotential (isothermal) surface causing the weakening of the wall-normal potential (temperature) gradient and, therefore, the local current density (heat flux). An additional point to be noted is that the intensification of the wall-normal gradients is the strongest where the curvature is the highest, thus suggesting that the wedge effect is strongly dependent on the shape of the interface. This is particularly true if, instead of a prismatic wedge, a pyramid or a cone is considered because, in the latter cases, also the direction orthogonal to the wedge of figure 23 has a curvature that further intensifies the electric field over the tip; this is usually referred to as the 'point effect' which is stronger than the wedge effect.

If now we reconsider the heat transfer problem in the light of the 'wedge effect', it is evident that a one-to-one comparison between different experiments is only possible within the same plate geometry even if the knowledge of the wedge effect provides us with a guideline for the interpretation of the differences among the published experiments. For example, the pyramids of Du & Tong (2000) having three-dimensional cusps, produce the highest intensification of the wall temperature gradient and therefore the strongest plume emission. This might explain why at $Ra \approx 10^3 Ra_{th}$, the increase of the Nusselt number is already $\sim$76 % with respect to the flat-plate case whereas for the present axisymmetric grooves it is only 35 %. On the other hand, the finite thermal conductivity of the plates of Du & Tong (2000) (made of brass) does not guarantee a constant temperature of the surface whose tips cool down (for the hot plate and vice versa for the cold one) under the effect of the enhanced heat transfer. This justifies the saturation of the $Nu\,vs.\,Ra$ power law to a smaller exponent as a balance between the plate effect (Chillà *et al.* 2004; Verzicco 2004; Brown *et al.* 2005) and the wall roughness. This conjecture is partly confirmed by the observation that Du & Tong (1998) for the flat plate give the correlation $Nu = 0.17Ra^{0.29}$ that at $Ra = 2 \times 10^{11}$ gives $Nu = 322$. When this value is corrected for the finite conductivity of the brass plates (whose thickness is assumed 5 %h), according to Verzicco (2004) we obtain $Nu_\infty = 423$ which is very close to the

value $Nu = 447 \pm 20$ of figure 5. On the other hand, Du & Tong (1998) measured for the rough plates $Nu = 0.30Ra^{0.29}$ that at $Ra = 2 \times 10^{11}$ gives $Nu = 568$. The same correction now yields $Nu_\infty = 747$ which is larger than the present value for grooved plates $Nu = 630 \pm 31$; should the correction be of the same order for smooth and rough plates, this difference of the Nusselt number would confirm the previous mentioned difference between 'wedge' and 'point effect' concerning the plume generation. We are aware, however, that there is no reason for the plate correction to be the same for smooth and rough plates and the previous result can only be taken as an encouraging indication. In order to understand this point better, *ad hoc* numerical simulations are being performed in which the thermal conductivity of the grooved plates is assigned and the results are compared with the present 'ideal' cases.

We are aware that the above discussion is rather speculative and that only the ongoing numerical simulations with finite thermal conductivity of the grooved plates can confirm or confute these ideas. However, Qiu *et al.* (2005) repeated the experiments of Du & Tong (2000) using pyramids directly machined from a solid copper plate instead of attaching pyramids machined from a brass plate over another brass plate. At ambient temperature, the thermal conductivity of pure copper is more than three times higher than that of brass and Qiu *et al.* (2005) observed an exponent $\beta = 0.35$ instead of the $\beta = 0.29$ of Du & Tong (2000). The value $\beta = 0.35$ is very close to the $\beta = 0.37$ our and the agreement is even more remarkable when considering the different geometry of the plates and the Prandtl number differing by about a factor of ten.

The results of Shen *et al.* (1996) are consistent with the above arguments since they used smaller pyramids than Du & Tong (2000), in an otherwise identical geometry, and they observed a Nusselt number increase of only 20 % beyond the transitional Rayleigh number. This can be understood considering that a roughness of smaller size yields a higher Ra_{th}, thus delaying the heat transfer increase. In contrast, the Nusselt number saturation caused by the finite conductivity of the plates depends mainly on the plate material which is the same (brass) in Shen *et al.* (1996) and Du & Tong (2000).

The results by Ciliberto & Laroche (1999) obtained by gluing glass spheres of identical diameter over copper plates gave the same $Nu\,vs.\,Ra$ power law as the smooth copper plates, but with a smaller absolute value of the Nusselt number. Since a layer of glass acts as an insulator, the connection of this problem to standard Rayleigh–Bénard convection might be questioned, nevertheless the decrease of the Nusselt number was probably caused by the poor thermal conductivity of the glass that completely made up for the enhanced plume emission from the top of the spheres. The generation of plumes from the spheres, in addition, is not as intense as in the previous experiments owing to the absence of sharp corners that produce strong wedge effects. In the case of multiple sphere diameters, the presence of different length scales spread the transition over a wide range of Rayleigh numbers and, as noted by Roche *et al.* (2001) this might mimic an increased exponent of the $Nu\,vs.\,Ra$ relation. Also in this case, however, the thermal conductivity of the spheres was too small to support the enhanced plume emission properly and the Nusselt number for the 'rough surface' was consistently smaller than for the same quantity over the smooth plates.

Roche *et al.* (2001) used axisymmetric grooves similar to the present ones for the plates and the sidewall and they obtained an increase of the exponent β in the $Nu\,vs.\,Ra$ power law up to $\beta = 0.51$. Their plates were made of oxygen-free pure copper that according to Verzicco (2004), in the case of a smooth surface for thicknesses of the order of 12.5 % of the plate distance h and using cryogenic gaseous

and liquid helium as the working fluid, are supposed to be free from finite conductivity effects up to $Ra \approx 10^{15}$. Although the presence of grooves might significantly alter this limit, the exponent increase was observed by Roche *et al.* (2001) in the range $10^{12} \leqslant Ra \leqslant 5 \times 10^{13}$, therefore, we still believe that the finite conductivity of the plates does not affect the results. The interpretation of the results by Roche *et al.* (2005) is more difficult since the same exponent $\beta = 1/2$ was found even in the case of brass plates whose thermal conductivity was about 250 times smaller than the copper reference plates (this value refers to the cryogenic temperatures of gaseous helium; at ambient temperature, the brass has a thermal conductivity of 1/2 to 1/3 of that of copper). Indeed, looking at the profiles of the surfaces (see figure 1 of Roche *et al.* 2005) it can be noted that the grooves are not exactly the same since in the copper plates they have the shape of 'rounded hills' while for the brass plates the shape seems to be a triangular saw tooth with a chopped top-hat tip. Given the sensitivity of the wedge effect to the surface geometry, it could be conjectured that the absence of sharp corners in the copper plates reduces the groove effect and this partially makes up for the better thermal conductivity with respect to the brass plates. It is worth mentioning, however, that the experiments by Roche *et al.* (2001, 2005) are the only ones performed at $Ra \geqslant 10^{12}$; in this range, the boundary layers are expected to undergo a turbulent transition and the mean flow structure, at least in a $\Gamma = 1/2$ cylindrical cell, is known to be different from that of the lower Rayleigh-number regimes (Stringano & Verzicco 2005). Within this scenario, it might be possible that the effect of the wall roughness is different from what has been described in the present paper and the results by Roche *et al.* (2001, 2005) cannot be discussed in a unified way. The fact that the roughness effect might be different is also suggested by the *Nu vs. Ra* relation (see figure 2 of Roche *et al.* 2005) showing exactly the same relation for copper and brass plates except for a reduction, although not systematic, of the Nusselt number for the brass plates limited to about 10 % over the whole range of *Ra*. On the other hand, the motivation of Roche *et al.* (2001, 2005) for using grooved plates was different from the other studies since it was intended only to disrupt the viscous sublayer of the turbulent boundary layer in order to cancel the logarithmic correction to the 1/2 power law of the *Nu vs. Ra* relation predicted by Kraichnan (1962).

According to the above discussion, the exponent $\beta = 1/2$ obtained with the axisymmetric simulations (figure 16) might not be related to the results of Roche *et al.* (2001) which were obtained in a completely different flow regime. As an aside, we note that in the axisymmetric flow, the presence of grooves completely changes the transition point since the heat transfer is similar to the values for the smooth plates up to $Ra \approx 10^9$ and then increases following the 1/2 power law, as can be seen from the compensated data of figure 16(*b*). The crossing, however, occurs at $Ra \approx 7 \times 10^9$ that, using the relation $\overline{\lambda}_\theta / h \simeq 1/(2Nu)$ yields $\overline{\lambda}_\theta / h \simeq 5.31 \times 10^{-3}$ which is about five times smaller than δ / h. This is caused by the flow symmetry which requires for the formation of a plume the simultaneous detachment of the thermal boundary layer along the whole circumference of the groove. This situation is clearly an artefact of the enforced symmetry and it is very different from the real three-dimensional flow where, although the preferred location for the plume formation remains the tips of the grooves, the former only covers a limited part of the groove and produce the classical mushroom-like structure driven by buoyancy (figure 24). This observation is fully confirmed by Sudhakar & Arakeri (2005) who report the formation of point plumes from the tips of their V-shaped straight grooves in contrast to the line plumes forming, in otherwise identical conditions, over smooth flat plates.

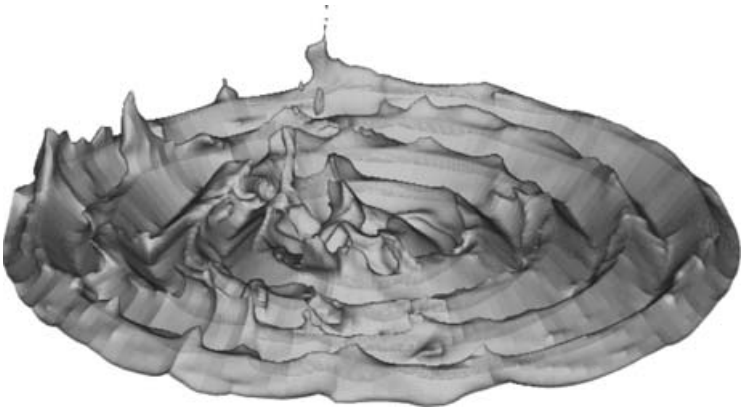

FIGURE 24. Instantaneous snapshot of a iso-temperature surface over the lower hot grooved plate ($\theta = 0.77$) at $Pr = 0.7$ and $Ra = 2 \times 10^{10}$.

From the above discussion, it is evident that the interaction between the heat transfer over non-flat plates and the thermal properties of the plate material is a key point for the correct comparison of different experiments and for the understanding of the heat transfer in real systems. For this reason, we are repeating the present numerical simulations considering different thermal conductivities of the plates. The results seem to support the present conclusions and a complete analysis will be presented in a forthcoming paper.

We wish to thank Dr P.–E. Roche, Professors P. Tong and J. Arakeri for fruitful discussions on an earlier version of this manuscript. The help of Professors F. Maradei and F. Lattarulo for clarifications on the wedge and point effects is also gratefully acknowledged. The simulation at the highest Rayleigh numbers were possible thanks to the computer facilities of CASPUR (Consorzio interuniversitario per le Applicazioni di Supercalcolo Per Università e Ricerca). Drs F. Massaioli and G. Amati are gratefully acknowledged for their continuous technical support. The paper was prepared with the financial support of CEMeC of Politecnico di Bari.

REFERENCES

AMIN, M. R. 1991 The effect of adiabatic wall roughness elements on natural convection heat transfer in vertical enclosures. *Intl J. Heat Mass Transfer* **34**, 2691–2701.

AMIN, M. R. 1993 Natural convection heat transfer and fluid flow in an enclosure convection heat transfer in vertical enclosures *Intl J. Heat Mass Transfer* **36** (10), 2707–2710.

ANDERSON, R. & BOHN, M. 1986 Heat transfer enhancement in natural convection enclosure flow. *J. Heat Transfer* **108**, 330–336.

BÉNARD, H. 1900 Les turbillons cellulaires dans une nappe liquide. *Rev. Gen. Sci. Pures Appl.* **11**, 1261–1271.

BROWN, E., NIKOLAENKO, A., FUNFSCHILLING, D. & AHLERS, G. 2005 Heat transport by turbulent Rayleigh–Bénard convection: effect of finite top and bottom plate conductivity. *Phys. Fluids*, **17**, 075108.

CAMUSSI, R. & VERZICCO, R. 2004 Temporal statistics in high Rayleigh number convective turbulence *Eur. J. Mech.* B/*Fluids* **23**, 427–442.

CASTAING, B., GUNARATNE, G., HESLOT, F., KADANOFF., L., LIBCHABER, A., THOMAE, S., WU, X. Z., ZALESKI, S. & ZANETTI, G. 1989 Scaling of hard thermal turbulence in Rayleigh–Bénard convection. *J. Fluid Mech.* **204**, 1–30.

Chavanne, X., Chillà, F., Castaing, B., Hebral, B., Chabaud, B. & Chaussy, J. 1997 Observation of the ultimate regime in Rayleigh–Bénard convection. *Phys. Rev. Lett.* **79**, 3648–3651.

Chavanne, X., Chillà, F., Chabaud, B., Castaing, B., Chaussy, J. & Hebral, B. 1996 High-Rayleigh-number convection with gaseous helium at low temperature. *J. Low Temp. Phys.* **104**, 109–129.

Chavanne, X., Chillà, F., Chabaud, B., Castaing, B. & Hebral, B. 2001 Turbulent Rayleigh-Bénard convection in gaseous and liquid He. *Phys. Fluids* **13**, 1300–1320.

Chillà, F., Rastello, M., Chaumat, S. & Castaing, B. 2004 Ultimate regime in Rayleigh–Bénard convection: the role of plates. *Phys. Fluids*, **16**, 2452–2456.

Ciliberto, S. & Laroche, C. 1999 Random roughness of boundary increases the turbulent scaling exponents. *Phys. Rev. Lett.* **82**, 3998–4001.

Cioni, S., Ciliberto, S. & Sommeria, J. 1997 Strongly turbulent Rayleigh–Bénard convection in mercury: comparison with results at moderate Prandtl number. *J. Fluid Mech.* **335**, 111–140.

Du, Y.–B. & Tong, P. 1998 Enhanced heat transport in turbulent convection over a rough surface. *Phys. Rev. Lett.* **81**, 987–990.

Du, Y.–B. & Tong, P. 2000 Turbulent thermal convection in a cell with ordered rough boundaries. *J. Fluid Mech.* **407**, 57–84.

Du, Y.–B. & Tong, P. 2001 Temperature fluctuations in a convection cell with rough upper and lower surfaces. *Phys. Rev.* E **63**, 046303.

Fadlun, E. A., Verzicco, R., Orlandi, P. & Mohd-Yusof, J. 2000 Combined immersed-boundary/finite-difference methods for three-dimensional complex flow simulations. *J. Comput. Phys.* **161**, 35–60.

Feder, J. 1988 *Fractals* Plenum Press.

Fujii, T., Fujii, M. & Takeuchi, M. 1973 Influence of various surface roughness on the natural convection. *Intl J. Heat Mass Transfer* **16**, 629–640.

Grossmann, S. & Lohse, D. 1991 Fourier–Weierstrass mode analysis for thermally driven turbulence. *Phys. Rev. Lett.* **67**, 445–448

Grossmann, S. & Lohse, D. 2000 Scaling in thermal convection: a unifying theory. *J. Fluid Mech.* **407**, 27–56.

Grossmann, S. & Lohse, D. 2001 Thermal convection for large Prandtl numbers. *Phys. Rev. Lett.* **86**, 3316–3319

Grötzbach, G. 1983 Spatial resolution requirements for direct numerical simulation of the Rayleigh–Bénard convection. *J. Comput. Phys.* **49**, 241–264.

Iaccarino, G. & Verzicco, R. 2003 Immersed boundary technique for turbulent flow simulations. *Appl. Mech. Rev.* ASME, **56**, 331–347.

Jiménez, J. 2004 Turbulent flows over rough walls. *Annu. Rev. Fluid Mech.* **36**, 173–196.

Kadanoff, L. 2001 Turbulent heat flow: structures and scaling. *Phys. Today* **54**, 34–39.

Kerr, R. 1996 Rayleigh number scaling in numerical convection. *J. Fluid Mech.* **310**, 139–179.

Kraichnan, R. H. 1962 Turbulent thermal convection at arbitrary Prandtl number. *Phys. Fluids* **5**, 1374–1389.

Malkus, M. V. R. 1954 Heat transport and spectrum of thermal turbulence. *Proc. R. Soc. Lond.* A **225**, 196.

Niemela, J. J., Skrbek., L., Sreenivasan, R. R. & Donnely, R. J. 2000 Turbulent convection at very high Rayleigh numbers. *Nature* **404**, 837–841.

Niemela, J. J. & Sreenivasan, K. R. 2003 Confined turbulent convection. *J. Fluid Mech.* **481**, 355–384.

Prasolov, R. S. 1961 On the effect of surface roughness on natural convection heat transfer from horizonthal cylinders to air. *Inzh. Fiz. Zh.* **4**, 3–7.

Qiu, X.-L., Xia, K.-Q. & Tong, P. 2005 Experimental study of velocity boundary layer near a rough conducting surface in turbulent natural convection. *J. Turb.* **6** (30), 1–13.

Rayleigh, Lord. 1916 On convective currents in a horizontal layer of fluid when the higher temperature is on the under side. *Phil. Mag.* **32**, 529–546.

Roche, P.-E., Castaing, B., Chabaud, B. & Hebral, B. 2001 Observation of the 1/2 power law in Rayleigh–Bénard convection. *Phys. Rev.* E **63**, 045303.

Roche, P.-E., Gauthier, F., Chabaud, B. & Hebral, B. 2005 Ultimate range of convection: robustness to poor thermal reservoirs. *Phys. Fluids* **17**, 115107.

Shen, Y., Xia K.-Q. & Tong, P. 1996 Turbulent convection over rough surfaces. *Phys. Rev. Lett.* **76**, 908–911.

Siggia, E. D. 1994 High Rayleigh number convection. *Annu. Rev. Fluid Mech.* **26**, 137–168.

Sini, J. F., Anquetin, S. & Mestayr, P. G. 1996 Pollutant dispersion and thermal effects in urban street canyons. *Atmos. Environ.* **30**, 2659–2677.

Stringano, G. & Verzicco, R. 2006 Mean flow structure in thermal convection in a cylindrical cell of aspect-ratio one half. *J. Fluid Mech.* **548**, 1–16.

Sudhakar, S. & Arakeri, J. 2005 Turbulent free convection over grooved surfaces. MSc thesis, Indian Institute of Science, Bangalore, India.

Swartzrauber, P. N. 1974 A direct method for the discrete solution of separable elliptic equations. *SIAM J. Numer. Anal.* **11**, 1136–1150.

Verzicco, R. 2002 Sidewall finite-conductivity effects in confined turbulent thermal convection *J. Fluid Mech.* **473**, 201–210.

Verzicco, R. 2003 Turbulent thermal convection in a closed domain: viscous boundary layer and mean flow effects. *Eur. Phys. J.* B **35**, 133–140.

Verzicco, R. 2004 Effects of non perfect thermal sources in turbulent thermal convection. *Phys. Fluids.* **16**, 1965–1979.

Verzicco, R. & Camussi, R. 2003 Numerical experiments on strongly turbulent thermal convection in a slender cylindrical cell. *J. Fluid Mech.* **477**, 19–49.

Verzicco, R. & Orlandi, P. 1996 A finite-difference scheme for three-dimensional incompressible flow in cylindrical coordinates. *J. Comput. Phys.* **123**, 402–413.

Villermaux, E. 1998 Transfer at rough sheared interfaces. *Phys. Rev. Lett.* **81**, 4859–4862.